

# Gyroscope-Like Complexes Based on Dibridgehead Diphosphine Cages That Are Accessed by Three-Fold Intramolecular Ring Closing Metatheses and Encase $\text{Fe}(\text{CO})_3$ , $\text{Fe}(\text{CO})_2(\text{NO})^+$ , and $\text{Fe}(\text{CO})_3(\text{H})^+$ Rotators

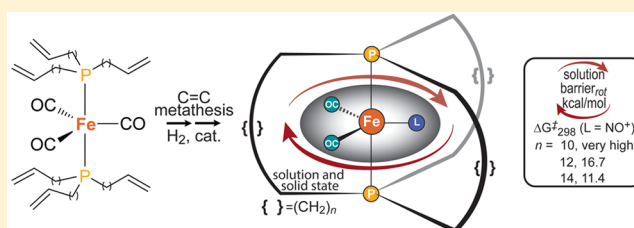
Georgette M. Lang,<sup>†</sup> Takanori Shima,<sup>‡</sup> Leyong Wang,<sup>‡</sup> Kyle J. Cluff,<sup>†</sup> Katrin Skopek,<sup>‡</sup> Frank Hampel,<sup>‡</sup> Janet Blümel,<sup>†</sup> and John A. Gladysz<sup>\*,†</sup>

<sup>†</sup>Department of Chemistry, Texas A&M University, PO Box 30012, College Station, Texas 77843-3012, United States

<sup>‡</sup>Institut für Organische Chemie and Interdisciplinary Center for Molecular Materials, Friedrich-Alexander-Universität Erlangen-Nürnberg, Henkestraße 42, 91054 Erlangen, Germany

## S Supporting Information

**ABSTRACT:** Reactions of  $\text{trans-Fe}(\text{CO})_3(\text{P}((\text{CH}_2)_m\text{CH}=\text{CH}_2)_3)_2$  ( $m = \text{a/4; b/5; c/6; e/8}$ ) and Grubbs' catalyst (12–24 mol %,  $\text{CH}_2\text{Cl}_2$ , reflux) give the cage-like trienes  $\text{trans-Fe}(\text{CO})_3(\text{P}((\text{CH}_2)_m\text{CH}=\text{CH}(\text{CH}_2)_m)_3)_2$  (**3a–c,e**, 60–81%). Hydrogenations ( $\text{CIRh}(\text{PPh}_3)_3$ , 60–80 °C) yield the title compounds  $\text{trans-Fe}(\text{CO})_3(\text{P}((\text{CH}_2)_n)_3)_2$  (**4a–c,e**, 74–86%;  $n = 2m + 2$ ), which have idealized  $D_{3h}$  symmetry. A crystal structure of **4c** suggests enough van der Waals clearance for the  $\text{Fe}(\text{CO})_3$  moiety to rotate within the three  $\text{P}(\text{CH}_2)_{14}\text{P}$  linkages; structures of  $E,E,E$ -**3a** show rotation to be blocked by the shorter  $\text{P}(\text{CH}_2)_4\text{CH}=\text{CH}(\text{CH}_2)_4\text{P}$  linkages. Additions of  $\text{NO}^+\text{BF}_4^-$  give the isoelectronic and isosteric cations  $[\text{Fe}(\text{CO})_2(\text{NO})(\text{P}((\text{CH}_2)_n)_3)]^+\text{BF}_4^-$  (**5a–c**<sup>+</sup> $\text{BF}_4^-$ ; 81–98%). Additions of  $[\text{H}(\text{OEt}_2)_2]^+\text{BAR}_f^-$  ( $\text{BAR}_f = \text{B}(3,5\text{-C}_6\text{H}_3(\text{CF}_3)_2)_4$ ) afford the metal hydride complexes  $\text{mer,trans-}[\text{Fe}(\text{CO})_3(\text{H})(\text{P}((\text{CH}_2)_n)_3)]^+\text{BAR}_f^-$  (**6a–c,e**<sup>+</sup> $\text{BAR}_f^-$ ; 98–99%). The behavior of the rotators in the preceding complexes is probed by VT NMR. At ambient temperature in solution, **5a,b**<sup>+</sup> $\text{BF}_4^-$  and **6a**<sup>+</sup> $\text{BAR}_f^-$  show two sets of  $\text{P}(\text{CH}_2)_{n/2}$   $^{13}\text{C}$  NMR signals (2:1), whereas **5c**<sup>+</sup> $\text{BF}_4^-$  and **6b,c**<sup>+</sup> $\text{BAR}_f^-$  show only one. At higher temperatures, the signals of **5b**<sup>+</sup> $\text{BF}_4^-$  coalesce; at lower temperatures, those of **5c**<sup>+</sup> $\text{BF}_4^-$  and **6b,c**<sup>+</sup> $\text{BAR}_f^-$  decoalesce. These data give  $\Delta H^\ddagger/\Delta S^\ddagger$  values (kcal/mol and eu) of 8.3/–28.4 and 9.5/–6.5 for  $\text{Fe}(\text{CO})_2(\text{NO})^+$  rotation (**5b,c**<sup>+</sup>) and 6.1/–23.5 for  $\text{Fe}(\text{CO})_3(\text{H})^+$  rotation (**6b**<sup>+</sup>).  $^{13}\text{C}$  CP/MAS NMR spectra show that the  $\text{Fe}(\text{CO})_3$  moiety in polycrystalline **4c** (but not **4a**) undergoes rapid rotation between –60 and 95 °C. Approaches to minimizing these barriers and developing molecular gyroscopes are discussed.



## INTRODUCTION

Molecular rotors<sup>1</sup> represent a large class of compounds with a variety of potentially practical functions.<sup>2–6</sup> They are often analyzed in the context of a rotator and a “stationary” stator. All motion is relative, so the latter is taken as the component with the greater moment of inertia.<sup>1</sup> There has been particular interest in developing molecular rotors that can structurally or functionally mimic various attributes of macroscopic gyroscopes.<sup>5–14</sup> The latter can be used to sense and/or maintain the orientations of diverse objects, with three representative examples that span more than a century of technology being torpedo warheads, space stations, and the displays associated with mobile phones.<sup>15</sup>

Some efforts involving molecular gyroscopes have been directed at engineering assemblies in which one or more components can exhibit rotation in the solid state, such as the amphidynamic crystals designed by Garcia-Garibay.<sup>5b</sup> Others have been concerned with rotation in solution or at solid/liquid interfaces, including ordered arrays constructed by mounting rotors on surfaces.<sup>16</sup> Importantly, all of the physics embodied in

macroscopic gyroscopes<sup>17</sup>—for example, the conservation of angular momentum—remains applicable at the molecular level,<sup>1</sup> thus setting the stage for the ultimate degree of miniaturization.

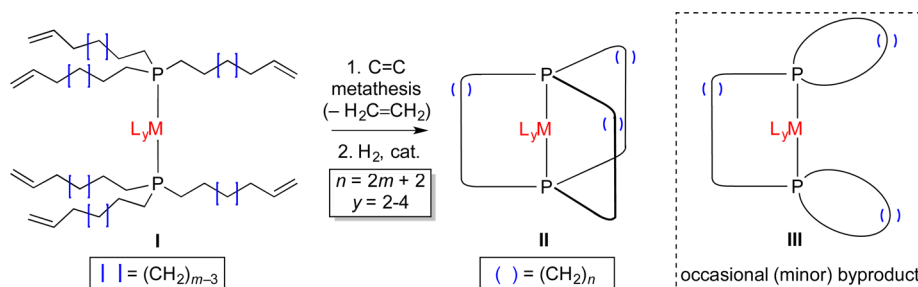
As shown in Scheme 1, we have discovered that 3-fold intramolecular ring closing metatheses *trans*-bis(phosphine) complexes of the type I can be effected in surprisingly high yields. This methodology has been applied to trigonal bipyramidal, square planar, and octahedral complexes, as detailed in a series of papers.<sup>7–12,14</sup> Subsequent hydrogenations afford adducts of cage-like macrocyclic dibridgehead diphosphines (II). These are reminiscent of a common type of macroscopic gyroscope in which the  $\text{ML}_y$  moiety substitutes for a flywheel. In some cases, an alternative product derived from a combination of inter- and intraligand metatheses has been detected (III) but is rarely the major species.<sup>8b,14</sup>

Depending upon the relative sizes of the macrocycles and the ligands  $\text{L}_y$  in II, rotation of the  $\text{ML}_y$  moiety may be possible.

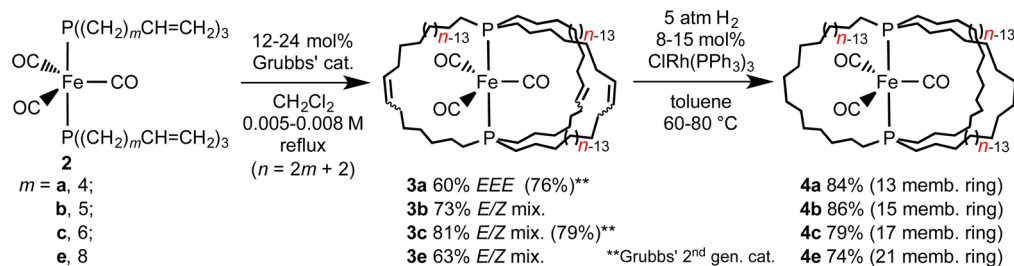
Received: March 28, 2016

Published: May 20, 2016

Scheme 1. General Synthetic Approach to Gyroscope-Like Complexes of Different Coordination Geometries



Scheme 2. Syntheses of Gyroscope-Like Iron Tricarbonyl Compounds



Interestingly, ligand substitutions can often be carried out in such environments,<sup>8–11,14a</sup> allowing the rotational barriers to be fine-tuned. The  $ML_y$  fragments can also be excised from the dibridgehead diphosphines under appropriate conditions.<sup>8,10b</sup> Furthermore, square planar palladium and rhodium systems can be effective catalyst precursors for carbon–carbon bond-forming reactions.<sup>10b</sup>

In this full paper, we return to the iron tricarbonyl systems disclosed in our initial communication<sup>7</sup> and provide complete details of their (1) syntheses, (2) substitution and addition reactions, (3) solid-state structures, and (4) rotational properties in solution and the solid state, as well as a variety of other phenomena. Together with the accompanying analyses, these data provide much new insight regarding the design and optimization of  $ML_y$ -based molecular gyroscopes. The syntheses of the requisite starting materials,  $trans\text{-Fe(CO)}_3\text{(P((CH}_2\text{)}_m\text{CH=CH}_2\text{))}_2$  (**2**;  $m = \text{a, 4; b, 5; c, 6; e, 8}$ ) have been detailed earlier.<sup>18</sup>

## RESULTS

**Syntheses of Title Complexes.** As shown in Scheme 2, a 0.0075 M  $\text{CH}_2\text{Cl}_2$  solution of **2a** was refluxed with Grubbs' catalyst.<sup>19a</sup> The loading, 13 mol %, represented 4 mol % per new C=C linkage. Workup afforded a homogeneous white solid in 60% yield. Aliquots from the reaction mixture were periodically assayed by  $^{31}\text{P}$  NMR and showed two intermediates, presumed to be monocyclic and bicyclic species. The chemical shifts moved progressively downfield as **2a** was converted to the product (64.2, 67.9, 75.0, 84.7 ppm,  $\text{C}_6\text{D}_6$ ).

The new complex and all others isolated below were characterized by IR and NMR ( $^1\text{H}$ ,  $^{13}\text{C}$ , and  $^{31}\text{P}$ ) spectroscopy and in most cases microanalyses and mass spectrometry. The mass spectrum exhibited an ion consistent with a 3-fold intramolecular metathesis product and no peaks of higher mass. A  $^{13}\text{C}$  NMR spectrum ( $\text{C}_6\text{D}_6$ ) indicated a highly symmetric product, with a single FeCO signal coupled to both phosphorus atoms (213.9 ppm,  $t$ ,  $^2J_{\text{CP}} = 28.1$  Hz), a single C=C signal (132.0 ppm), and four  $\text{CH}_2$  signals (24.3 to 33.4 ppm). Hence, the new complex was assigned the gyroscope-like structure  $E,E,E\text{-3a}$  depicted in Scheme 2, with three 13-membered rings

containing  $E$  C=C linkages, as verified crystallographically below.

A toluene solution of  $E,E,E\text{-3a}$  was then treated with  $\text{H}_2$  (5 atm) in the presence of Wilkinson's catalyst ( $\text{ClRh(PPh}_3\text{)}_3$ ; 15 mol %) at 80 °C. Workup gave the hydrogenation product  $trans\text{-Fe(CO)}_3\text{(P((CH}_2\text{)}_{10}\text{)}_3\text{P)}$  (**4a**) as a white solid in 84% yield. The  $^{13}\text{C}$  NMR spectrum ( $\text{C}_6\text{D}_6$ ) exhibited one FeCO signal (216.4 ppm,  $t$ ,  $^2J_{\text{CP}} = 28.0$  Hz) and five  $\text{CH}_2$  signals (21.2 to 29.1 ppm), consistent with the idealized molecular symmetry ( $D_{3h}$ ). When aliquots from the reaction mixture were assayed by  $^{31}\text{P}$  NMR, two intermediates, presumed to be diolefinic and monoolefinic species, were detected. The chemical shifts moved progressively upfield as  $E,E,E\text{-3a}$  was converted to **4a** (84.7, 81.1, 78.1, 75.5 ppm,  $\text{C}_6\text{D}_6$ ). Complexes  $E,E,E\text{-3a}$  and **4a** were moderately air-sensitive but showed no mass loss at temperatures lower than 300 °C (TGA).

The generality of this sequence was tested with **2b,c,e** (Scheme 2), which contain longer methylene segments. Similar metatheses gave **3b,c,e**, featuring three 15-, 17-, and 21-membered rings, in 63–81% yields. Mass spectra showed molecular ions and no peaks of higher mass. However, mixtures of  $E/Z$  C=C isomers formed, as evidenced by multiple  $^{31}\text{P}$  NMR signals and more complex patterns of  $\text{CH=CH}$   $^1\text{H}$  NMR signals. High  $E$  selectivities as seen with  $E,E,E\text{-3a}$  appear limited to ring closing metatheses that place  $trans$  P–M–P linkages in 13-membered rings.<sup>20</sup> In any event, when **3b,c,e** were hydrogenated with Wilkinson's catalyst, isomerically homogeneous **4b,c,e** were obtained in 74–86% yields.

Superior yields are often obtained with advanced generations of Grubbs' catalysts. When **2a,c** and Grubbs' second-generation catalyst<sup>19b</sup> were similarly reacted, the yield of  $E,E,E\text{-3a}$  increased from 60 to 76%, but that of **3c** was scarcely affected. In efforts with related complexes to date, only one other example has been found where Grubbs' second-generation catalyst afforded a significantly higher yield. This case also involved a 13-membered ringed product.<sup>20</sup>

The spectroscopic properties of **4a–c,e** exhibited several trends. The  $^{31}\text{P}$  NMR signals shifted ca. 10 ppm upfield as the ring sizes increased, consistent with data for other cyclic

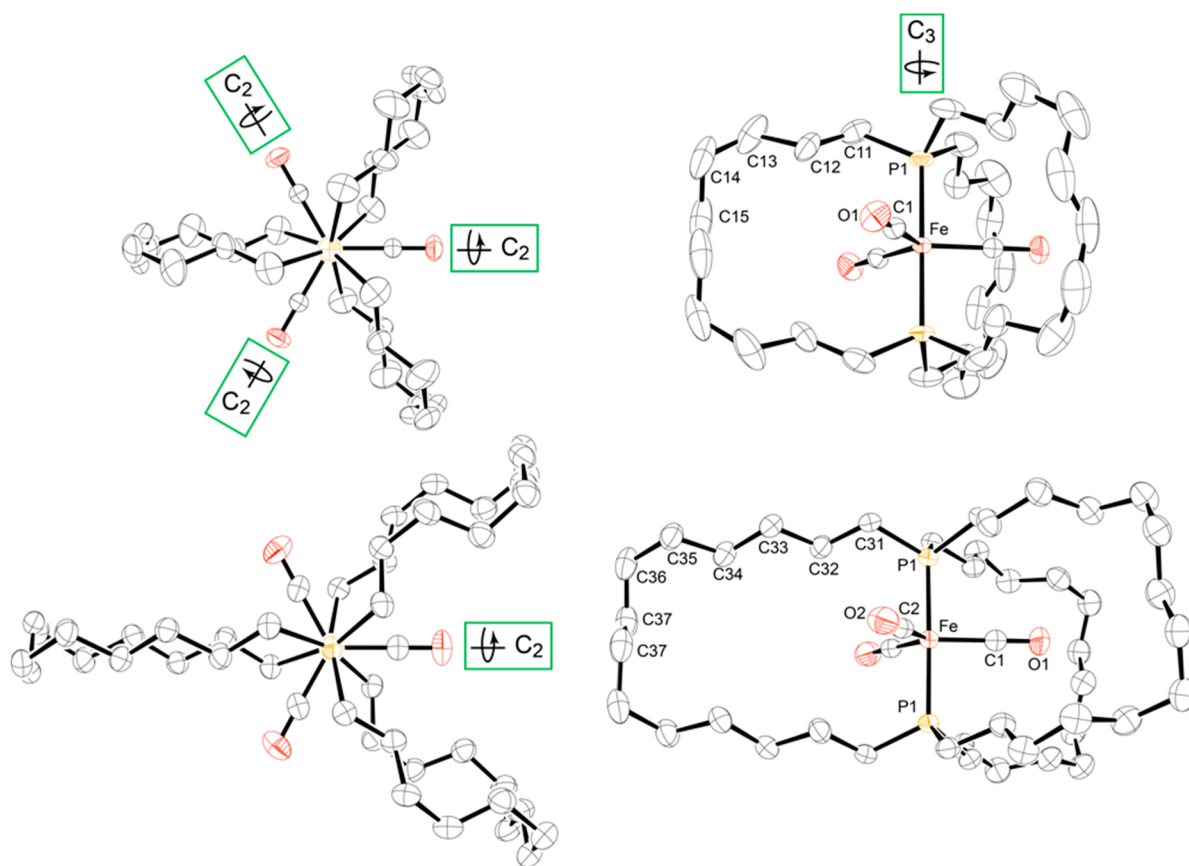


**Figure 1.** Molecular structures of  $E,E,E$ -3a·C<sub>6</sub>H<sub>6</sub> (top) and 4c (bottom) with solvate molecules and hydrogen atoms omitted and attendant symmetry axes depicted.

organophosphorus compounds.<sup>21</sup> The IR  $\nu_{\text{CO}}$  values of the complexes with the two smaller ring sizes (4a,b; 1841, 1853 cm<sup>-1</sup>) were at lower frequencies than the others (4c,e; 1861, 1859 cm<sup>-1</sup>). However, the <sup>13</sup>C NMR chemical shifts and <sup>2</sup>J<sub>CP</sub> values for the CO signals fell into narrow ranges (216.4, 215.5, 215.6, 215.7 ppm, C<sub>6</sub>D<sub>6</sub>; 27.5, 28.4, 29.0, 28.0 Hz). The PCH<sub>2</sub>, PCH<sub>2</sub>CH<sub>2</sub>, and PCH<sub>2</sub>CH<sub>2</sub>CH<sub>2</sub> signals were apparent doublets of doublets (30.1–32.0 ppm, <sup>1</sup>J<sub>CP</sub> = 14.7–15.0, 11.7–12.1 Hz),<sup>22</sup> singlets (21.2–24.3 ppm), and virtual triplets (29.1–31.6 ppm, <sup>3</sup>J<sub>CP</sub> = 5.3–7.2 Hz),<sup>22</sup> respectively, as confirmed by <sup>1</sup>H, <sup>1</sup>H COSY and <sup>1</sup>H, <sup>13</sup>C HSQC experiments.<sup>23</sup>

**Molecular Structures.** To help analyze the steric environments within the diphosphine cages, structural data for the preceding compounds were sought. Accordingly, crystals of the benzene and mesitylene solvates  $E,E,E$ -3a·C<sub>6</sub>H<sub>6</sub> and  $E,E,E$ -3a·2(1,3,5-C<sub>6</sub>H<sub>3</sub>(CH<sub>3</sub>)<sub>3</sub>), as well as nonsolvated 4c, were grown. X-ray data were collected, and the structures were solved as summarized in the Experimental Section and Table S1.

Thermal ellipsoid diagrams of two representative complexes,  $E,E,E$ -3a·C<sub>6</sub>H<sub>6</sub> and 4c, are presented in Figure 1. Complex  $E,E,E$ -3a·C<sub>6</sub>H<sub>6</sub> exhibited a 3-fold symmetry axis coincident with the P–Fe–P linkage and (in a perpendicular plane) three 2-fold symmetry axes coincident with each Fe–C–O linkage (see Figure 1; point group D<sub>3h</sub>). The C<sub>3</sub> axis also passed through the centroid of the benzene solvate. Complex 4c exhibited a C<sub>2</sub> axis coincident with the Fe–C1–O1 linkage, and  $E,E,E$ -3a·2(1,3,5-C<sub>6</sub>H<sub>3</sub>(CH<sub>3</sub>)<sub>3</sub>) was of analogous symmetry. In all complexes, the substituents along the P–Fe–P axes (CH<sub>2</sub>/CO/CH<sub>2</sub>) adopted staggered conformations (Figure 1, left). Crystallographic distances of greatest interest are summarized

in Table 1. The bond lengths and angles about iron are close to those of other *trans*-bis(phosphine) iron tricarbonyl complexes.<sup>24</sup>

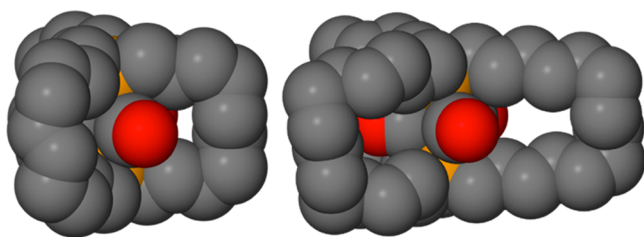
Space-filling representations of the preceding structures are given in Figure 2. It is evident that the Fe(CO)<sub>3</sub> moiety of  $E,E,E$ -3a is essentially in a straight jacket, such that each carbonyl group can only oscillate between two of the *trans*-spanning carbon chains, each part of a 13-membered ring. For more quantitative analyses, the radius of the Fe(CO)<sub>3</sub> rotator must be considered. This can be calculated by taking the average iron–oxygen distance<sup>25</sup> and adding the van der Waals (vdW) radius of oxygen.<sup>26</sup> As outlined in Table 1, the resulting value, 4.45 Å, is compared with the distances between the iron atom and the C=C carbon atoms of the three *trans*-spanning linkages (5.343–5.345 Å), which are the atoms closest to the plane of the rotator. The van der Waals radius of a carbon atom<sup>26</sup> is then subtracted from the shortest of the six values to give 3.64 Å (see “Fe–C<sub>distal</sub>–vdW”). This can be taken as a clearance for the rotator, somewhat analogous to a bridge height on a highway. Obviously, it is impossible for a rotator of radius 4.45 Å to pass underneath a bridge height of 3.64 Å.

In contrast to the situation with  $E,E,E$ -3a, the space-filling representations of 4c suggest that there is enough room for the Fe(CO)<sub>3</sub> moiety to rotate within the three P(CH<sub>2</sub>)<sub>14</sub>P linkages, each part of a 17-membered ring. Here, the carbon atoms closest to the plane of the rotator are methylene groups, and their distances from iron span a considerable range (6.64–7.86 Å) because of conformational differences in the macrocycles. When the van der Waals radius of a carbon atom is subtracted from these values, considerable clearance remains (4.45 Å vs

**Table 1.** Intramolecular and Intermolecular Distances Involving Rotator and Stator Atoms in Gyroscope-Like Complexes (Å) and Selected Bond and Torsion Angles (deg)

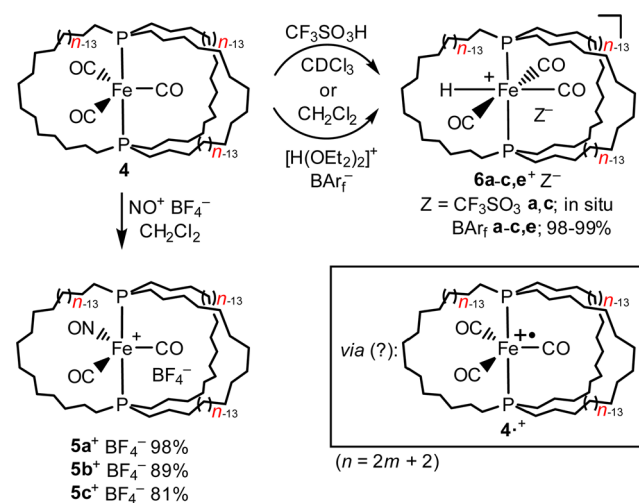
complex	<i>E,E,E</i> -3a·C <sub>6</sub> H <sub>6</sub>	<i>E,E,E</i> -3a·2(1,3,5-C <sub>6</sub> H <sub>3</sub> (CH <sub>3</sub> ) <sub>3</sub> )	4c
Fe–P <sup>a</sup>	2.190	2.202	2.206
FeCO <sup>a</sup>	2.929	2.928	2.927
radius of rotator <sup>b</sup>	4.45	4.45	4.45
Fe–C <sub>a</sub> <sup>c</sup>	5.34	5.32	7.46
Fe–C' <sub>a</sub> <sup>c</sup>	5.34	5.33	6.64
Fe–C <sub>b</sub> <sup>c</sup>	5.34	5.33	6.64
Fe–C' <sub>b</sub> <sup>c</sup>	5.34	5.32	7.46
Fe–C <sub>c</sub> <sup>c</sup>	5.35	5.31	7.86
Fe–C' <sub>c</sub> <sup>c</sup>	5.35	5.31	7.86
Fe–C <sub>distal</sub> –vdW <sup>d</sup>	3.64	3.61	4.94
Fe–C <sub>distal</sub> '–vdW <sup>e</sup>	3.65	3.63	6.16
Fe–C <sub>neighbor</sub> <sup>f</sup>	5.87	6.10 <sup>g</sup>	6.04
Fe–C <sub>neighbor</sub> –vdW <sup>h</sup>	4.17	4.40 <sup>g</sup>	4.34
∠ P–Fe–P	180.0	179.8	178.9
P(C <sub>6</sub> H <sub>5</sub> ) <sub>3</sub> /P(C <sub>6</sub> H <sub>3</sub> ) <sub>3</sub> <sup>i</sup>	5.94	5.94	6.00
C <sub>a</sub> P–Fe–PC <sub>a</sub> <sup>j</sup>	6.02	6.06	6.13
C <sub>b</sub> P–Fe–PC <sub>b</sub>	6.02	6.06	6.13
C <sub>c</sub> P–Fe–PC <sub>c</sub>	6.02	6.09	6.02
C <sub>a</sub> P–Fe–PC <sub>b</sub> <sup>k</sup>	6.35	6.26	6.42
C <sub>b</sub> P–Fe–PC <sub>c</sub>	6.35	6.29	6.36
C <sub>c</sub> P–Fe–PC <sub>a</sub>	6.35	6.29	6.36
C <sub>a</sub> –P–P–C <sub>a</sub> <sup>l</sup>	34.3	44.4	38.0
C <sub>b</sub> –P–P–C <sub>b</sub>	34.3	44.4	38.0
C <sub>c</sub> –P–P–C <sub>c</sub>	34.5	44.5	38.3
C <sub>a</sub> –P–P–C <sub>b</sub> <sup>m</sup>	85.7	75.3	82.6
C <sub>b</sub> –P–P–C <sub>c</sub>	85.6	75.7	81.6
C <sub>c</sub> –P–P–C <sub>a</sub>	85.6	75.7	81.6

<sup>a</sup>Average distance within the molecule. <sup>b</sup>FeCO distance plus the van der Waals radius of the oxygen atom (1.52 Å). <sup>c</sup>Distance from iron to the two remote carbon atoms of the three macrocycles (a, b, c; c always contains a C<sub>2</sub> axis) that are closest to the plane of the rotator (Fe–C<sub>distal</sub>). <sup>d</sup>Shortest of the previous six distances, minus the van der Waals radius of the carbon atom (1.70 Å). <sup>e</sup>Longest of the previous six distances, minus the van der Waals radius of the carbon atom. <sup>f</sup>Distance from iron to the nearest carbon atom of a neighboring gyroscope-like or solvate molecule. <sup>g</sup>This distance is for a solvate molecule; it is 0.58 Å further to the nearest carbon atom of another molecule of *E,E,E*-3a. <sup>h</sup>Previous entry minus the van der Waals radius of the carbon atom. <sup>i</sup>Distance between planes defined by the three carbon atoms attached to each phosphorus atom (see VI in Figure 10 below). <sup>j</sup>Distance between the PCH<sub>2</sub> carbon atoms of each macrocycle (see IX in Figure 10). <sup>k</sup>Distance between the PCH<sub>2</sub> carbon atoms that most closely flank each CO ligand (from different macrocycles; see VII and VIII in Figure 10). <sup>l</sup>C–P–P–C torsion angle within the three macrocycles (a, b, c). <sup>m</sup>C–P–P–C torsion angle involving carbon atoms that most closely flank each CO ligand (from different macrocycles).

**Figure 2.** Space filling representations of *E,E,E*-3a·C<sub>6</sub>H<sub>6</sub> (left) and 4c (right) with solvate molecules and hydrogen atoms omitted.

4.94–6.10 Å). Usually, the shortest (rotation limiting) distance is emphasized; however, other approaches to analyzing these data are possible.<sup>27</sup> Additional aspects of these crystal structures, including properties associated with the lattice, are analyzed in the following sections and in the [Supporting Information](#).

**Substitutions and Oxidations.** The symmetries of *E,E,E*-3a and 4a–c,e are too high to probe the rate of Fe(CO)<sub>3</sub> rotation by conventional solution-phase NMR techniques. One of the three trans-spanning linkages or carbonyl ligands must be differentiated. It has been shown that reactions of the bis(phosphine) tricarbonyl complexes *trans*-Fe(CO)<sub>3</sub>(PR<sub>3</sub>)<sub>2</sub> and NO<sup>+</sup>Z<sup>–</sup> (Z = BF<sub>4</sub> and PF<sub>6</sub>) give salts of the isoelectronic and

**Scheme 3.** Substitution and Addition Reactions Involving Gyroscope-Like Complexes 4

isosteric dicarbonyl nitrosyl cations, *trans*-[Fe(CO)<sub>2</sub>(NO)(PR<sub>3</sub>)<sub>2</sub>]<sup>+</sup>Z<sup>–</sup>, in near quantitative yields.<sup>28</sup> As depicted in Scheme 3, reactions of 4a–c and NO<sup>+</sup>BF<sub>4</sub><sup>–</sup> gave the dicarbonyl nitrosyl

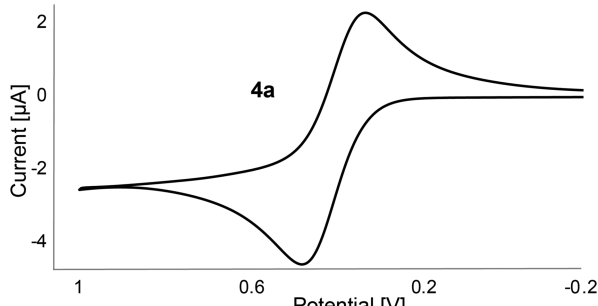


complexes  $[trans\text{-Fe}(\text{CO})_2(\text{NO})(\text{P}((\text{CH}_2)_n)_3\text{P})]^+\text{BF}_4^-$  (**5a-c** $^+\text{BF}_4^-$ ) in 81–98% yields after workup.

The IR spectra of **5a-c** $^+\text{BF}_4^-$  exhibited two  $\nu_{\text{CO}}$  bands (2023–2030  $\text{cm}^{-1}$  m, 1953–1965  $\text{cm}^{-1}$  s) and a  $\nu_{\text{NO}}$  band (1752–1764  $\text{cm}^{-1}$  s). Ambient-temperature  $^{13}\text{C}$  NMR spectra of **5a,b** $^+\text{BF}_4^-$  showed two sets of  $\text{P}(\text{CH}_2)_{n/2}$  signals with an area ratio of ca. 2:1, whereas the spectrum of **5c** $^+\text{BF}_4^-$  gave only one set. This indicates, in accord with the expectations from the crystal structures, that  $\text{Fe}(\text{CO})_2(\text{NO})^+$  rotation is rapid on the NMR time scale at room temperature for **5c** $^+\text{BF}_4^-$  (17-membered rings) but slow for **5a,b** $^+\text{BF}_4^-$  (13- and 15-membered rings; two  $(\text{CH}_2)_n$  chains occupy interstices between the CO/NO ligands and the third the interstice between two CO ligands. Importantly, the  $\text{PCH}_2\text{CH}_2\text{CH}_2$  and CO signals of **5c** $^+\text{BF}_4^-$  retain phosphorus couplings, excluding dissociation of the carbon monoxide ligand or phosphorus donor atoms in the mechanisms that render the bridges equivalent.

From a steric standpoint, it is curious that these carbonyl ligand substitutions are not inhibited by the three methylene bridges. In this context, note that  $\text{NO}^+$  is a strong one electron oxidant<sup>29</sup> and that 17-valence-electron metal complexes show enhanced substitution labilities.<sup>30</sup> Thus, cyclic voltammograms of *E,E,E*-**3a** and **4a-c** were recorded under standard conditions in  $\text{CH}_2\text{Cl}_2$ . As summarized in Table 2, all exhibited appreciably

Table 2. Cyclic Voltammetry Data for Iron Tricarbonyl Complexes<sup>a</sup>



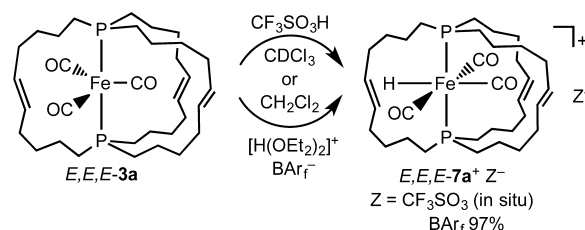
complex	$E_{\text{p,a}}$ (V)	$E_{\text{p,c}}$ (V)	$E^\circ$ (V)	$\Delta E$ (mV)	$i_{\text{c}}/i_{\text{a}}$
<i>E,E,E</i> - <b>3a</b>	0.342	0.215	0.279	127	0.950
<b>4a</b>	0.477	0.335	0.406	142	0.918
<b>4b</b>	0.438	0.209	0.324	229	0.887
<b>4c</b>	0.461	0.166	0.314	295	0.921

<sup>a</sup>Conditions: 0.0010 M in 0.10 M  $\text{Bu}_4\text{N}^+\text{PF}_6^-/\text{CH}_2\text{Cl}_2$ ,  $22 \pm 1^\circ\text{C}$ ; Pt working and auxiliary electrodes and Ag/AgCl pseudoreference; scan rate, 200 mV/s (data were similar at 100 and 150 mV/s); ferrocene = 0.46 V. All scans were continued to  $-1.0$  V, but no additional features were observed.

reversible one-electron oxidations with  $i_{\text{c}}/i_{\text{a}}$  values of 0.89–0.95. For **4a** through **4c**, the  $E^\circ$  values monotonically decreased from 0.406 to 0.314 V (vs ferrocene at 0.46 V). This indicates thermodynamically more favorable oxidations or phosphine ligands that are progressively more  $\sigma$ -donating and/or less  $\pi$ -accepting. Since under similar conditions the  $\text{NO}^+/\cdot\text{NO}$  couple has a redox potential of 1.00 V,<sup>29c</sup> quantitative generation of the radical cations **4a-c** $^+$  (Scheme 3) is possible.

**Protonations.** Additional derivatives of lower symmetry were sought. Iron complexes of the formula  $trans\text{-Fe}(\text{CO})_3(\text{PR}_3)_2$  have been protonated by a variety of strong acids (HZ), affording octahedral cationic hydride complexes  $mer,trans\text{-}[\text{Fe}(\text{CO})_3(\text{H})(\text{PR}_3)_2]^+\text{Z}^-$ .<sup>31</sup> As shown in Schemes 3 and 4, **4a,c** and *E,E,E*-**3a** were combined with  $\text{CF}_3\text{SO}_3\text{H}$  in  $\text{CDCl}_3$  in NMR tubes. The hydride

Scheme 4. Protonation of *E,E,E*-**3a**



complexes  $mer,trans\text{-}[\text{Fe}(\text{CO})_3(\text{H})(\text{P}((\text{CH}_2)_n)_3\text{P})]^+\text{CF}_3\text{SO}_3^-$  (**6a,c** $^+\text{CF}_3\text{SO}_3^-$ ) and *E,E,E-mer,trans*- $[\text{Fe}(\text{CO})_3(\text{H})(\text{P}((\text{CH}_2)_4\text{CH}=\text{CH}(\text{CH}_2)_4)_3\text{P})]^+\text{CF}_3\text{SO}_3^-$  (*E,E,E*-**7a** $^+\text{CF}_3\text{SO}_3^-$ ) formed in quantitative yields, as evidenced by diagnostic  $^1\text{H}$  NMR signals ( $-9.41$  to  $-9.46$  ppm,  $t$ ,  $^2J_{\text{HP}} = 21.4$  to  $29.4$  Hz). However, workups of these triflate salts did not give solid products, and the attendant data are provided in the Supporting Information.

Thus, larger scale reactions were conducted with **4a-c,e** or *E,E,E*-**3a** and the protic oxonium salt  $[\text{H}(\text{OEt}_2)_2]^+\text{BARf}^-$  ( $\text{BARf}^- = \text{B}(3,5\text{-C}_6\text{H}_3(\text{CF}_3)_2)_4^-$ ).<sup>32</sup> Workups gave the hydride complexes **6a-c,e** $^+\text{BARf}^-$  and *E,E,E*-**7a** $^+\text{BARf}^-$  in 97–99% yields as powders or gums. Interestingly, the  $^2J_{\text{HP}}$  values associated with the  $\text{FeH}$   $^1\text{H}$  NMR signals increased with macrocycle size (22.1–22.7, 27.0, 30.2, and 32.2 Hz). As seen for **4a-c,e**, the  $^{31}\text{P}$  NMR signals of **6a-c,e** $^+\text{BARf}^-$  shifted upfield as the ring sizes increased ( $\Delta\text{ppm}$  ca. 17). In accord with literature precedent,<sup>31</sup> three IR  $\nu_{\text{CO}}$  bands were observed, with the intensities decreasing with increasing frequency.<sup>33</sup> All bands were at higher frequencies than those of the neutral precursors.

The ambient-temperature  $^{13}\text{C}$  NMR spectra of **6a** $^+\text{Z}^-$  ( $\text{Z} = \text{CF}_3\text{SO}$  and  $\text{BARf}$ ) and **7a** $^+\text{CF}_3\text{SO}_3^-$ , which have 13-membered rings, exhibited two sets of  $\text{P}(\text{CH}_2)_4\text{C}$  signals (all 2:1). This indicates, analogous to the case with the nitrosyl complex **5a** $^+\text{BF}_4^-$ , that  $\text{Fe}(\text{CO})_3(\text{H})^+$  rotation is slow on the NMR time scale. The complexes **6b** $^+\text{BARf}^-$  and **6c** $^+\text{Z}^-$ , which have 15- or 17-membered rings, showed only a single set of  $\text{CH}_2$  signals, suggesting rapid rotation. Importantly, the hydride  $^1\text{H}$  NMR signals retained phosphorus couplings ( $t$ ,  $^2J_{\text{HP}} = 28\text{--}29$  Hz), indicating that the hydride and phosphorus donor atoms remain bound during the process that renders the bridges equivalent. Similarly, the CO signals retained phosphorus couplings ( $t$ ,  $^2J_{\text{CP}} = 15\text{--}20$  Hz).

**Lattice Analyses.** The relationships between molecular rotors in crystal lattices is of interest from a variety of standpoints. In the case of **4c**, the molecules pack in well-defined layers with all P–Fe–P axes parallel, as shown in Figure 3 (top). Between adjacent and all subsequent layers, the P–Fe–P axes are offset. Within a layer, the molecules exhibit two orientations, as shown in Figure 3 (bottom). One carbonyl oxygen atom of each rotator “points” at the middle or innermost  $\text{CH}_2\text{CH}_2$  linkage of a 17-membered ring of an adjacent molecule. The other two carbonyl oxygen atoms are directed more toward the centers of 17-membered rings of adjacent molecules.

As shown in Figure 4, the solvate *E,E,E*-**3a**· $\text{C}_6\text{H}_6$  packs in stacks in which the benzene molecules are sandwiched between the P–Fe–P axes. Within each stack, the rotators and stators of adjacent molecules are antiparallel. The individual molecules in adjacent stacks are offset, with the P–Fe–P units somewhat higher or lower (Figure 4). Hence, there is no layering as observed with **4c**. However, all of the P–Fe–P axes remain parallel. The lattice of *E,E,E*-**3a**· $2(1,3,5\text{-C}_6\text{H}_3(\text{CH}_3)_3)$ , depicted

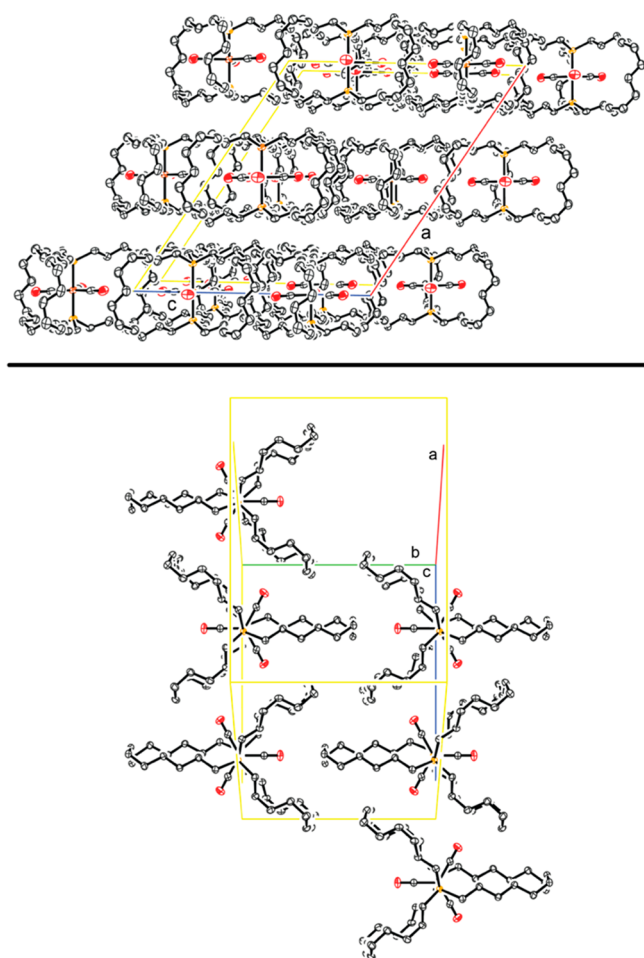


**Figure 3.** Crystal lattice of **4c** viewed along (top) and perpendicular (bottom) to the *b* axis; Fe = orange dots and O = red dots.

in Figures S1 and S2, is somewhat more complex. The mesitylene solvent molecules are  $\pi$ -stacked in pairs (vertical separation 3.9 Å) and do not sandwich individual iron complexes as in *E,E,E*-**3a**·C<sub>6</sub>H<sub>6</sub>.

An important issue regarding the viabilities of such crystalline iron complexes as molecular gyroscopes involves the distances of neighboring molecules from the rotators. Of particular interest are cases where the distances from the iron atom of one molecule to the nearest non-hydrogen atoms of neighboring molecules (adjusted for the van der Waals radii of the nearest atoms) are greater than the radius of the rotator. These would be the most promising candidates for rotation in the solid state. Relevant data, derived from the crystal structures, are presented in Table 1 (see “Fe–C<sub>neighbor</sub>–vdW”). Importantly, the distances are quite close in **4c** (4.34 Å vs 4.45 Å rotator radius). However, as shown in Figure S3, this atom is considerably removed from the plane of the rotator. The next nearest atom, which is only slightly removed from the rotator plane, allows for more clearance (4.53 Å after vdW correction). The comparisons are similarly auspicious for the solvates of *E,E,E*-**3a**, but the rotators therein are constrained by the shorter P(CH<sub>2</sub>)<sub>4</sub>CH=CH(CH<sub>2</sub>)<sub>4</sub>P bridges (see “Fe–C<sub>distal</sub>–vdW”).

**Variable-Temperature and Solid-State NMR Experiments.** As shown in Figure 5 (left), <sup>13</sup>C NMR spectra of **5c**<sup>+</sup>BF<sub>4</sub><sup>−</sup> were recorded in CDFCl<sub>2</sub> at progressively lower temperatures (−10 to −80 °C). The chemical shifts of the PCH<sub>2</sub>CH<sub>2</sub>CH<sub>2</sub> carbon atoms remained roughly constant ( $\Delta\delta$  0.3–0.6 ppm),

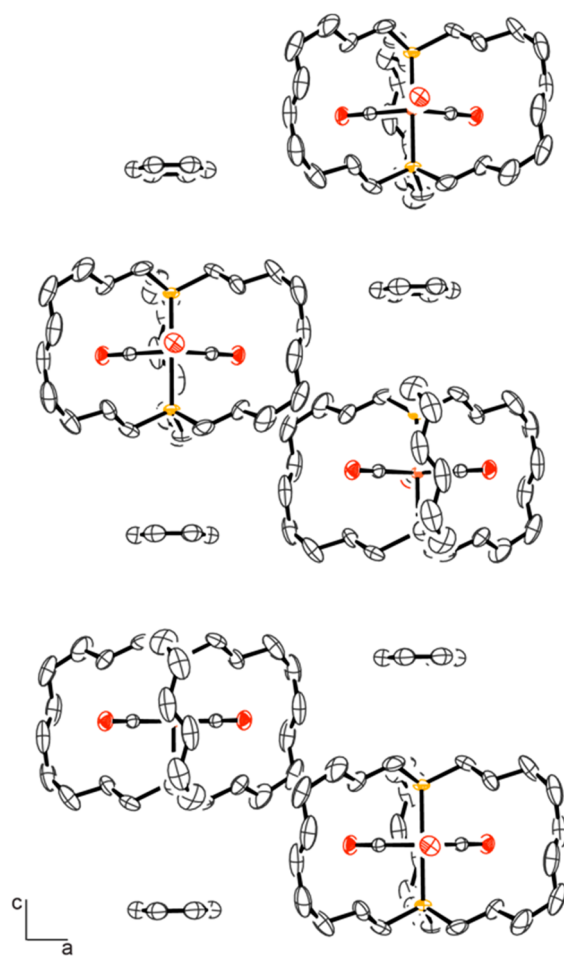


**Figure 4.** Crystal lattice of *E,E,E*-**3a**·C<sub>6</sub>H<sub>6</sub> as viewed along the *b* axis.

whereas some of the others varied much more ( $\Delta\delta$  1.3–2.1 ppm). This suggests that the methylene groups that are not anchored as closely to the phosphorus atoms can sample conformations with greater chemical shift differences, the differential entropies of which in turn lead to more pronounced temperature dependencies. In any event, many peaks broadened, and the PCH<sub>2</sub>CH<sub>2</sub> signal (green) eventually decoalesced in a reasonably well-defined manner (two peaks, ca. 2:1 area ratio). The line shapes were simulated using gNMR (red)<sup>35</sup> and the rate constants extrapolated at each temperature.

An Eyring plot using these rate constants (Figure s4) gave  $\Delta H^\ddagger$  and  $\Delta S^\ddagger$  values of 9.5 kcal/mol and −6.5 eu for the process rendering the CH<sub>2</sub> signals equivalent. This was attributed to rotation of the Fe(CO)<sub>2</sub>(NO)<sup>+</sup> moiety, as detailed further in the Discussion section.

Next, <sup>13</sup>C NMR spectra of **5b**<sup>+</sup>BF<sub>4</sub><sup>−</sup>, which features smaller 15-membered rings, were recorded in C<sub>6</sub>D<sub>5</sub>Cl at progressively higher temperatures (23–100 °C). All of the CH<sub>2</sub> signals broadened, and as depicted in Figure 5 (middle), two (ca. 2:1 area ratio; P(CH<sub>2</sub>)<sub>*n*'</sub>CH<sub>2</sub>, *n*' ≥ 3) exhibited a well-defined coalescence at 80 °C. The data were treated as for **5c**<sup>+</sup>BF<sub>4</sub><sup>−</sup>, with an Eyring plot (Figure s5) giving  $\Delta H^\ddagger$  and  $\Delta S^\ddagger$  values of 8.3 kcal/mol and −28.4 eu. This corresponds to a  $\Delta G^\ddagger_{298\text{ K}}$  value of 16.7 kcal/mol, which as expected is a considerably higher barrier than that of **5c**<sup>+</sup>BF<sub>4</sub><sup>−</sup> (11.4 kcal/mol). Additional aspects of the activation parameters are analyzed in the Discussion section.

Finally, <sup>13</sup>C NMR spectra of **6b**<sup>+</sup>BAr<sub>f</sub><sup>−</sup>, which features a tetra-substituted rotator, were recorded in CD<sub>2</sub>Cl<sub>2</sub> at progressively

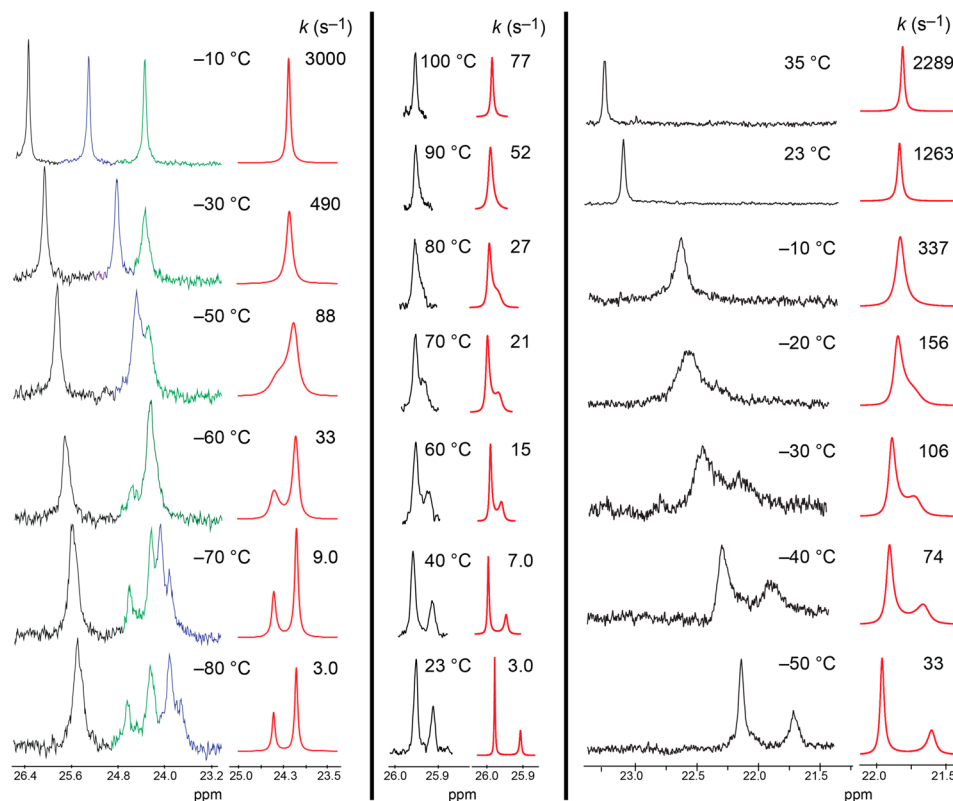


**Figure 5.** Partial  $^{13}\text{C}$  NMR spectra of  $5\text{c}^+\text{BF}_4^-$  ( $\text{CDFCl}_2$ , left),  $5\text{b}^+\text{BF}_4^-$  ( $\text{C}_6\text{D}_5\text{Cl}$ , middle), and  $6\text{b}^+\text{BAr}_f^-$  ( $\text{CD}_2\text{Cl}_2$ , right) as a function of temperature. Each spectrum is paired with simulated line shapes for the signals of interest (red).

lower temperatures (35 to  $-50^\circ\text{C}$ ). As depicted in Figure 5 (right), the  $\text{PCH}_2\text{CH}_2$  signal broadened and then decoalesced into two peaks (ca. 2:1 area ratio). A similar treatment of these data (Figure S6) gave  $\Delta H^\ddagger$  and  $\Delta S^\ddagger$  values of 6.1 kcal/mol and  $-23.5$  eu for the process that renders the  $\text{CH}_2$  signals equivalent (discussion section). This corresponds to a  $\Delta G^\ddagger_{298\text{ K}}$  value of 13.0 kcal/mol.

Rotational barriers were probed in the solid state<sup>36</sup> using polycrystalline **4c**. A  $^{13}\text{C}$  CP/MAS (cross-polarization, magic angle spinning) NMR spectrum was recorded at ambient temperature ( $25^\circ\text{C}$ ), as depicted in Figure 6. As expected, the  $(\text{CH}_2)_{14}$  signals

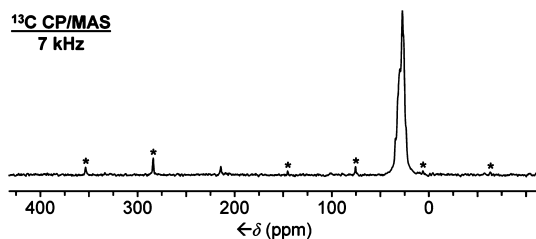


**Figure 6.**  $^{13}\text{C}$  CP/MAS NMR spectrum of polycrystalline **4c**; asterisks denote rotational sidebands of the CO signal.

overlapped and did not show a large chemical shift anisotropy (CSA)<sup>37,38</sup> when the rotational speed was 7 kHz. However, the CO  $^{13}\text{C}$  signal, which was visible at 214.4 ppm, exhibited the characteristic large carbonyl CSA<sup>37–39</sup> with the parameters<sup>40</sup>  $\delta_{11} = 367.2$ ,  $\delta_{22} = 352.1$ , and  $\delta_{33} = -76.2$  ppm, and a span<sup>38</sup>  $\delta_{11}-\delta_{33}$  of 443.4 ppm.<sup>40</sup> The residual line width of the CO signal was only 76 Hz, and the line was highly symmetric with no indication of a signal splitting or shoulder. In view of the unit cell of **4c** (Figure 3), multiple isotropic signals, representing the

different orientations of the CO groups with respect to the external magnetic field, would have been expected for a static  $\text{Fe}(\text{CO})_3$  moiety. Since the  $^{13}\text{C}$  CP/MAS spectrum exhibited only one narrow line for all the CO ligands, it can be concluded that the  $\text{Fe}(\text{CO})_3$  unit is rotating rapidly about the P–Fe–P axis within the  $(\text{CH}_2)_{14}$  linkages. The shape and line width of the isotropic line of the CO signal did not change upon heating or cooling the sample from 95 to  $-60^\circ\text{C}$ . Hence, rotation is rapid over the entire temperature range.

In contrast, the CO signal of polycrystalline **4a** exhibited a much broader isotropic line with a width of 231 Hz. The unsymmetric shape of the signal indicates the presence of several slightly different isotropic lines, speaking for a static  $\text{Fe}(\text{CO})_3$  unit in the solid state.

As shown in Figure 7,  $^{31}\text{P}$  CP/MAS NMR spectra of polycrystalline **4c** were recorded under static conditions (wide-line spectrum, bottom) and at 4 and 7 kHz rotational frequencies. A signal with an isotropic chemical shift of 72.1 ppm exhibited a CSA characteristic of gyroscope-like molecules with  $\text{Fe}(\text{CO})_3$  rotators<sup>41</sup> with the parameters<sup>40</sup>  $\delta_{11} = 130.4$ ,  $\delta_{22} = 117.4$ , and  $\delta_{33} = -31.4$  ppm and a span<sup>38</sup> of  $\delta_{11}-\delta_{33}$  of 161.8 ppm.<sup>40</sup> The residual line width of the isotropic signal was only 141 Hz; however, the resonance appeared slightly unsymmetric. A negative linebroadening factor revealed the presence of two overlapping signals with nearly identical chemical shifts. This is in accord with the crystal lattice of **4c** (Figure 3), which shows that there are two magnetically inequivalent phosphorus nuclei in the unit cell.

## DISCUSSION

**Syntheses.** Scheme 2 establishes that trigonal bipyramidal gyroscope-like complexes with iron tricarbonyl rotators are easily



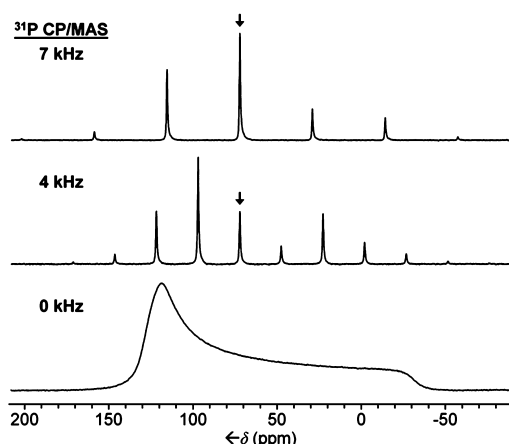


**Figure 7.**  $^{31}\text{P}$  CP/MAS NMR spectra of **4c** at the indicated rotational speeds; the arrows denote the isotropic lines.

accessed via 3-fold intramolecular ring closing metatheses involving trans phosphine ligands of the formula  $\text{P}((\text{CH}_2)_m\text{CH}=\text{CH}_2)_3$  with  $m \geq 4$ . The overall yields for the metathesis/hydrogenation sequences range from 47 to 64%. These are distinctly higher than those for educts with square planar or octahedral coordination geometries,<sup>11,14</sup> which require values of  $m \geq 6$  and are presumed to give higher fractions of oligomeric or polymeric products. Furthermore, with some square planar complexes,<sup>8</sup> minor amounts of byproducts with the connectivity **III** (Scheme 1) can be observed. For a few of the octahedral complexes, these dominate.<sup>14</sup>

These differences are likely associated with the conformational energy minima of the precursors. For the tricarbonyl complexes **2a–c,e**, one would expect the  $(\text{CH}_2)_m\text{CH}=\text{CH}_2$  substituents on each phosphorus atom to be staggered with respect to the CO ligands on iron, as shown in **IV** in Figure 8. This preorganizes the educt for intramolecular and interligand metathesis. Once one macrocycle has been generated, the reduced P–Fe–P conformational mobility should further favor intramolecular over intermolecular metathesis. However, there is no marked cooperativity because each successive macrocyclization can be observed by  $^{31}\text{P}$  NMR (see above).

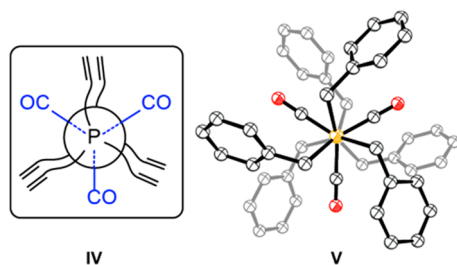


**Figure 8.** Newman type projection (**IV**) showing the conformational “preorganization” for 3-fold intramolecular and interligand C=C metathesis in **2a–c,e** and a crystal structure of a bis(tribenzylphosphine) analog (**V**).

We were unable to crystallize any of the complexes corresponding to **IV**. However, the crystal structure of a bis(tribenzylphosphine) analog, depicted in Figure 8 (**V**), has been reported.<sup>24</sup> This clearly exhibits staggered relationships between the phosphorus and iron substituents. These orientations are largely retained in the crystalline gyroscope-like complexes (Figure 1). In any case, square planar and octahedral educts do

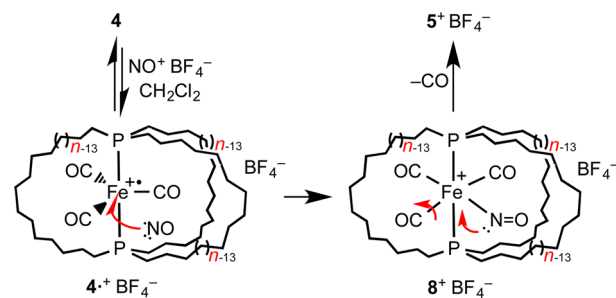
not provide analogous conformational templates, as illustrated elsewhere.<sup>8b,14a</sup> Thus, yields for the metathesis/hydrogenation sequences are lower, and products with 13- and 15-membered rings cannot be accessed at all. Furthermore, the greater number of rotator substituents in the octahedral precursors can impede interligand metathesis, increasing the relative amounts of byproducts **III**.<sup>14</sup>

In general, internal olefins are much less reactive toward chain-carrying ruthenium alkylidene catalysts than terminal olefins.<sup>42</sup> For this and other reasons, we consider the ring closing metatheses of **2a–c,e** to be under kinetic control. Insightful recent studies have described methods for minimizing oligomeric byproducts.<sup>43</sup> Thus, it may prove possible to further increase the yields in Scheme 2. Indeed, in a previous paper involving dimacrocyclic complexes with P–Pt–P linkages, we were able to vary the ratios of monomeric/oligomeric products by carrying out metatheses at different concentrations using Grubbs’ second-generation catalyst.<sup>20</sup>

As noted above, only in the case of *E,E,E*-**3a** was the ring closing metathesis highly stereoselective. Interestingly, ring closing metatheses of other complexes with *trans*- $\text{H}_2\text{C}=\text{CH}(\text{CH}_2)_4\text{P}-\text{M}-\text{P}(\text{CH}_2)_4\text{CH}=\text{CH}_2$  linkages give exclusively *E* C=C isomers, at least within the limits of detection.<sup>20,44</sup> In this context, note that an *E* C=C segment spans a carbon–carbon distance of 3.9 Å, whereas a *Z* segment extends only 3.15 Å.<sup>45</sup> Hence, despite the higher strain energy associated with *E* C=C moieties in smaller carbocyclic rings, this stereochemistry provides more “rope” for bridging a fixed distance and may be the more stable isomer in the absence of transannular interactions or other destabilizing features. Indeed, for an olefinic 14-membered lactone synthesized using Grubbs’ second-generation catalyst, a 12:1 *E/Z* ratio has been reported, close to the 19:1 equilibrium value derived computationally.<sup>46</sup>

**Reactions of Gyroscope-Like Complexes.** The cage-like diphosphine ligands in *E,E,E*-**3a** and **4a–c,e** would not be expected to significantly hinder the protonations in Schemes 3 and 4. However, the substitution of a CO ligand by the cation of  $\text{NO}^+\text{BF}_4^-$  is another matter. As noted above,  $\text{NO}^+$  is a strong one-electron oxidant,<sup>29</sup> and the generation of 17-valence-electron radical cations  $4^+\text{BF}_4^-$  (Scheme 3) is thermodynamically downhill. Although such species are substitution labile,<sup>30</sup> we suggest that it is more probable at least for the larger ring sizes that the resulting  $\cdot\text{NO}$  radical covalently binds to give 18-valence-electron octahedral species  $8^+\text{BF}_4^-$  shown in Scheme 5. The nitrogen lone pair associated with the bent nitrosyl ligand would then serve as an internal nucleophile for displacing a carbonyl ligand.

**Scheme 5.** One Possible Mechanism for the Substitution of CO by  $\text{NO}^+$  in **4**



Given the extensive chemistry of iron carbonyl complexes, there are many possible reactions that could be carried out with



the products in Schemes 2–4. Some negative results not treated in the Results section are briefly summarized here. First, attempts to replace one or more of the CO ligands in *E,E,E*-3a by the ligand-based C=C linkages were unsuccessful, either under photochemical conditions (450 W ultraviolet lamp through quartz; sun lamp through Pyrex) or using chemical agents such as  $\text{Me}_3\text{N}^+-\text{O}^-$ .<sup>47</sup> When the reaction of 4c and  $\text{Me}_3\text{N}^+-\text{O}^-$  was monitored by  $^{31}\text{P}$  NMR, a new signal could be detected, but subsequent additions of potential ligands did not give tractable products.

Well-defined reactions of methyl iodide and *trans*- $\text{Fe}(\text{CO})_3(\text{PMe}_3)_2$  have been reported,<sup>48</sup> but 4c gave no conversion under comparable conditions over a 10 day period. Although MeLi readily adds to  $\text{Fe}(\text{CO})_5$  in ether at  $-60^\circ\text{C}$ ,<sup>49</sup> no reaction was detected when 4c and MeLi were combined in THF- $d_8$  at  $66^\circ\text{C}$ , as assayed by NMR ( $^{31}\text{P}$ ,  $^1\text{H}$ , and  $^{13}\text{C}$ ; 1–24 h). Cationic complex  $5c^+\text{BF}_4^-$  should be more electrophilic. However, no reaction took place when a  $\text{CD}_2\text{Cl}_2$  solution of  $5c^+\text{BF}_4^-$  was treated with the strong hydride donor  $\text{K}(\text{sec-Bu})_3\text{BH}$  or formyl complex  $(\eta^5\text{-C}_5\text{H}_5)\text{Re}(\text{PPh}_3)(\text{NO})(\text{CHO})$ .<sup>50,51</sup> Since analogous results were obtained with *trans*- $[\text{Fe}(\text{CO})_2(\text{NO})(\text{P}((\text{CH}_2)_m\text{CH}=\text{CH}_2)_3)]^+\text{BF}_4^-$ ,<sup>18</sup> which lacks the cage-like diphosphine ligand, this cannot be attributed to a steric effect.

**Rotator and Stator Dimensions.** Figure 9 provides a graphical representation of some of the metrical data in Table 1. The radii of the  $\text{Fe}(\text{CO})_3$  rotators (4.45 Å) are easily calculated as described above.<sup>25</sup> However, the interior dimensions of the stator are more challenging to define. As is evident from the many crystallographically characterized gyroscope-like complexes<sup>8,10,11,14a</sup> and 4c in this paper, the macrocycles can sample many conformations and do not necessarily extend to an equal extent from

the metal center. Thus, per Figure 9, we consider the two carbon atoms in each trans-spanning linkage that lie nearest to the plane of the rotator.

For the complexes in this paper, these are the innermost  $\text{CH}_2\text{CH}_2$  or  $\text{CH}=\text{CH}$  segments. In contrast, in other complexes the macrocycle conformations are not necessarily symmetric with respect to the plane of the rotator, such that the in-plane  $\text{CH}_2\text{CH}_2$  segments can become biased toward one phosphorus terminus.<sup>8,10,11,14a</sup> In any event, we commonly focus on the shortest of the six iron–carbon distances. After subtraction of the van der Waals radius of carbon, this gives the most conservative estimate of the void space or horizontal clearance. However, it could be argued that average values would provide better comparisons between complexes in solution.

Empirically, we find that when the radius of the rotator is less than or approximately equal to the horizontal clearance, rotation is rapid in solution at room temperature on the NMR time scale. We note in passing that this treatment neglects the hydrogen atoms associated with the trans-spanning linkages. However, it is often found that the sizes of hydrogen atoms are negligible when evaluating the feasibility of dynamic processes from space-filling models.

Importantly, the void space within the diphosphine cage is three-dimensional, and the “vertical” or “top/bottom” clearance also affects rotational barriers. Figure 10 focuses on the spatial relationship between the CO ligands and the C–P–Fe–P–C linkages. One obvious reference point is the distance between the planes defined by the three carbon atoms attached to each phosphorus atom, which are constrained to be parallel by virtue of the  $\text{C}_2$  symmetry axes noted above (5.94–6.00 Å per Table 1 and VI in Figure 10). Another would be the distances between the  $\text{PCH}_2$  carbon atoms within each macrocycle—i.e., those with the smallest C–P–P–C torsion angles (see IX in Figure 10). As would be expected from the diagonal relationships of the atoms with respect to the P–Fe–P vectors, the distances are slightly greater than the plane–plane separations, and in 4c, these range from 6.02 to 6.13 Å (Table 1). From either reference point, subtraction of the van der Waals radii of two carbon atoms gives a vertical clearance (2.62–2.73 Å for 4c). The distances between the  $\text{PCH}_2$  carbon atoms that most closely flank each CO ligand in the crystal can also be considered (VII and VIII in Figure 10). Since these involve different macrocycles, they are somewhat greater (6.36–6.42 Å for 4c).

What counts now in the vertical dimension is not the radius of the rotator, but its fatness, which is best approximated by the van der Waals diameter of the ligating carbon, 3.40 Å. This is

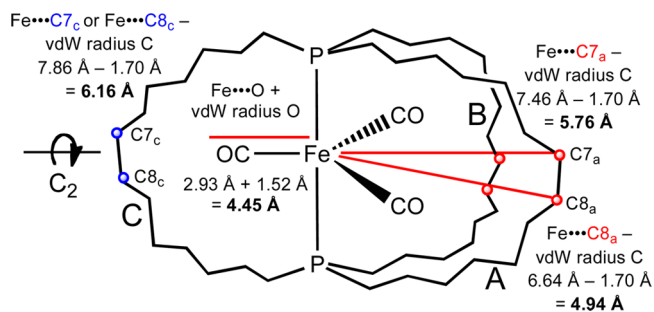


**Figure 9.** Spatial relationships involving the iron atom, rotator, and  $(\text{CH}_2)_{14}$  bridges in 4c; see text and Table 1 (vdW = van der Waals; A/B/C refer to the macrocycle labels in Table 1).

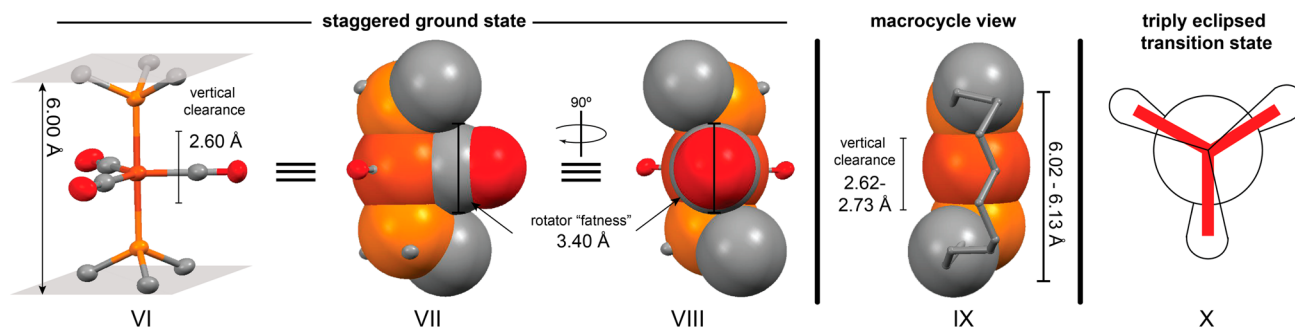


**Figure 10.** Steric relationships between atoms in 4c relevant to “vertical clearance” of the rotator. VI: separation of planes defined by the  $\text{PCH}_2$  carbon atoms. VII and VIII: as in VI, but with selected atoms at van der Waals radii (e.g., the  $\text{PCH}_2$  carbon atoms that most closely flank a CO ligand, which are from different macrocycles). IX: relationship of the two  $\text{PCH}_2$  carbon atoms within a macrocycle. X: Newman-type projection of transition state in which all three CO ligands pass between  $\text{PCH}_2$  carbon atoms belonging to the same macrocycle.

somewhat greater than the distance between the flanking PCH<sub>2</sub> carbon atoms in the crystal, minus their van der Waals radii (6.36–6.42 Å – 2(1.70 Å) or 2.96–3.02 Å for **4c**; see VII and VIII). In the transition state X, the three CO ligands are positioned between PCH<sub>2</sub> carbon atoms of the type in IX, with narrower clearances (2.62–2.73 Å for **4c**). This squeeze can to some extent be ameliorated by concurrent conformational changes within the macrocycles. These would, for example, expand key torsion angles and/or increase rotator/stator clearances. Regardless, this analysis shows that there is the potential to significantly lower rotational barriers by increasing the distance between the metal and the bridgehead donor atoms that anchor the cage-like ligand. Some opportunities are detailed below.

**Rotational Barriers.** As represented by X in Figure 10, the transition state for rotator rotation in trigonal bipyramidal gyroscope-like complexes entails a 3-fold eclipsing interaction. As illustrated in Figure 11 and elsewhere,<sup>8b,14a</sup> the corresponding transition states for octahedral or square planar gyroscope-like complexes involve only a single eclipsing interaction. For this and other reasons, these barriers are much lower, as long as the ligands on the rotators have approximately the same sizes (CO ~ Cl ~ CH<sub>3</sub>). Although activation parameters are not yet available, it has been possible to bound the barrier for Rh(CO)<sub>2</sub>I rotation as substantially greater than that of Rh(CO)(I).<sup>10a</sup>

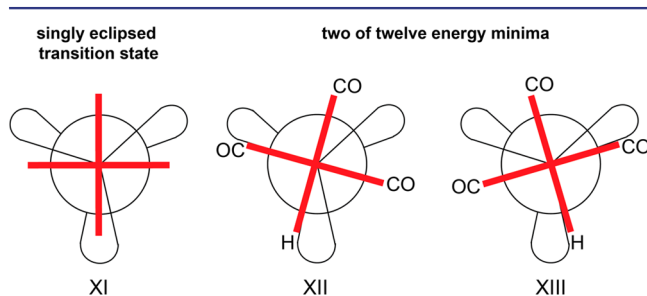


**Figure 11.** Selected rotator conformations in octahedral gyroscope-like complexes such as **6b**<sup>+</sup>BAr<sub>f</sub><sup>−</sup>.

The variable-temperature NMR data in Figure 5 allow rotational barriers to be calculated for the dicarbonyl nitrosyl complexes **5b,c**<sup>+</sup>BF<sub>4</sub><sup>−</sup>. The  $\Delta G^\ddagger_{298\text{ K}}$  values, 16.7 and 11.4 kcal/mol, respectively, exhibit the expected decrease with increased macrocycle size. The cations of these salts are viewed as isoelectronic and isosteric surrogates for the tricarbonyl complexes **4b,c**, which are presumed to have very similar barriers.

The negative  $\Delta S^\ddagger$  values (−28.4 and −6.5 eu) are consistent with the loss of entropy that would be anticipated from the 3-fold eclipsing interaction in X and correlated changes in the macrocycle conformations to alleviate the interactions diagrammed in Figure 10. However, the  $\Delta H^\ddagger$  values counterintuitively increase with increased macrocycle size (8.3 and 9.5 kcal/mol). In this context, note that the  $\Delta S^\ddagger$  values also increase (becoming less negative). This logically follows from the much higher degree of correlated conformational changes that would be required for the three CO ligands to pass through the smaller macrocycles in **5b**<sup>+</sup>BF<sub>4</sub><sup>−</sup> as opposed to those in **5c**<sup>+</sup>BF<sub>4</sub><sup>−</sup>. Thus, at least for this pair of complexes, there is appreciable enthalpy–entropy compensation.<sup>52</sup> One consequence is an isokinetic temperature of −217 °C (56 K), but under experimentally relevant conditions, Fe(CO)<sub>2</sub>(NO)<sup>+</sup> rotation is always faster in **5c**<sup>+</sup>BF<sub>4</sub><sup>−</sup>.

To render the signals of all three P(CH<sub>2</sub>)<sub>n</sub>CH<sub>2</sub> carbon atoms of **5b,c**<sup>+</sup>BF<sub>4</sub><sup>−</sup> equivalent, the Fe(CO)<sub>2</sub>(NO)<sup>+</sup> moieties must rotate by 240° (all CH<sub>2</sub> groups need to exchange between

CO/NO and CO/CO environments). In the case of **5c**<sup>+</sup>BF<sub>4</sub><sup>−</sup>, the rate constant for this process can be extrapolated from the Eyring plot (Figure S4) as 25 600 s<sup>−1</sup> (Hz) at 25 °C. When this is scaled to 360°, it represents a rate equivalent to 1 000 000 rpm at room temperature. However, Fe(CO)<sub>2</sub>(NO)<sup>+</sup> rotation is not unidirectional but Brownian, a topic further treated in the final section.

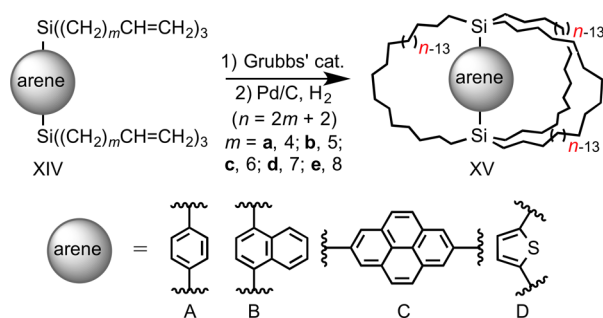
Solid-state NMR data can supply information on the rotational barriers of the more symmetric tricarbonyl complexes **4a–c,e**. Interestingly, since only a single symmetric CP/MAS CO <sup>13</sup>C NMR signal with a narrow line width is observed with crystalline **4c**, the barrier to Fe(CO)<sub>3</sub> rotation appears to be lower than that for Fe(CO)<sub>2</sub>(NO)<sup>+</sup> rotation in **5c**<sup>+</sup>BF<sub>4</sub><sup>−</sup> in solution. This is supported by the CP/MAS data for **4a**, which show two overlapping CO signals. Thus, **4c** affords amphidynamic crystals, with the rotator able to navigate past atoms of neighboring molecules in the solid state and surmount the intramolecular van der Waals interactions diagrammed in Figure 10. A DSC analysis of **4c** revealed a melting exotherm (160 °C) but no other phase transitions down to −100 °C. In contrast, **4b**, which should have a higher barrier to Fe(CO)<sub>3</sub> rotation, exhibited a second phase transition at a temperature lower than the melting endotherm (−1 °C vs 231 °C).

As noted above, the transition state for rotation of the rotator in analogous octahedral gyroscope-like complexes features only a single eclipsing interaction, as shown in XI in Figure 11. Thus, it is not surprising that **6b**<sup>+</sup>BAr<sub>f</sub><sup>−</sup> exhibits a lower rotational barrier than **5b**<sup>+</sup>BF<sub>4</sub><sup>−</sup>, given the equal macrocycle sizes ( $\Delta G^\ddagger_{298\text{ K}}$  13.0 vs 16.7 kcal/mol). However, additional subtle points merit emphasis. For example, in view of the symmetry of **6b**<sup>+</sup>BAr<sub>f</sub><sup>−</sup> (see representative rotamer XII), three sets of CH<sub>2</sub> signals would be expected (1:1:1) as opposed to the two observed (2:1). Several rhodium complexes behave similarly, all of which feature a single small ligand on the rotator that is able to rapidly pass through a macrocycle on the NMR time scale.<sup>9,10</sup> In the case of **6b**<sup>+</sup>BAr<sub>f</sub><sup>−</sup>, the barrier for the hydride ligand passing through a macrocycle would be expected to be much lower than those for a CO ligand. Thus, the interconversion of the pseudomirror image rotamers XII and XIII could remain rapid at the low temperature limit in Figure 5, resulting in two sets of CH<sub>2</sub> signals. As more fully analyzed elsewhere,<sup>14a,57</sup> such complexes exhibit 12 maxima (and minima) as the rotator is rotated through 360°; for a CH<sub>2</sub> group to sample all environments, the rotator must traverse 330°.

In these contexts, the contributions of other research groups merit emphasis. First, Setaka has utilized 3-fold intramolecular ring closing metatheses to access a number of systems that feature an arene rotator with two silicon substituents connected by three polymethylene bridges.<sup>6</sup> Representative examples are shown in Scheme 6. He has determined a variety of rotational barriers by NMR, both in solution (XV-Bc,d using variable temperature EXSY <sup>13</sup>C NMR spectra)<sup>6a,d</sup> and the solid state (XV-Aa,c,e using <sup>2</sup>H NMR spectra).<sup>6c</sup> Paralleling our observations, the solid-state barriers are quite low ( $E_a$  6.6–9.0 kcal/mol), despite van der Waals interactions between the rotator and stator. Kono has also probed these barriers computationally.<sup>53</sup>

Garcia-Garibay has used other synthetic methods to access carbocyclic analogs of XV and versions with ether containing polymethylene segments.<sup>54</sup> He has determined rotational barriers in the solid state for a variety of *p*-phenylene or diadamantane rotators suspended between two bulky (triarylmethyl)ethynyl or steroidal end groups, using <sup>2</sup>H NMR and variable-temperature <sup>13</sup>C CP/MAS NMR.<sup>5a,c,55</sup>

**Scheme 6. Organosilicon Gyroscope-Like Compounds Prepared by the Setaka Group**



**Toward Molecular Gyroscopes.** With either macroscopic or molecular gyroscopes, the minimization of friction is an important operational consideration. Toward this end, the analyses presented above point to a number of ways that the stators in **4**,  $5^+\text{BF}_4^-$ , and  $6^+\text{Z}^-$  can be further optimized. Perhaps the most obvious would be to substitute the iron–phosphorus bonds by iron–arsenic or osmium–phosphorus bonds. Since these involve heavier elements, they should be 3–5% longer,<sup>14a,56</sup> leading to more vertical clearance for the rotator (Figure 10). Unfortunately, we have not yet been able to prepare osmium analogs of  $5\text{c}^+\text{BF}_4^-$ , although analogs of **4c** are readily available.<sup>14a</sup> Arsenic analogs will be described in a forthcoming publication.<sup>57</sup> Another strategy, reminiscent of a theme in Garcia-Garibay's efforts, would involve trans alkynyl ligands that would space the atoms that anchor the polymethylene chains further from the metal.

With regard to the horizontal dimension of the stator, the incorporation of rigid units such as *p*-phenylene ( $\text{C}_6\text{H}_4$ ) or polyynediyl ( $-(\text{C}\equiv\text{C})_n-$ ) moieties near the anchoring heteroatom might enforce a minimum extension for each macrocycle. Rigid units in any position will also reduce conformational degrees of freedom and possibly lead to less negative  $\Delta S^\ddagger$  values (lower  $\Delta G^\ddagger$  values). In terms of optimizing the rotator, hydride ligands are particularly svelte.<sup>4f</sup> With a rotator of formula  $\text{M}(\text{H})_y$ , barriers might be probed in solution by lowering the symmetry of the stator.

In all of the phenomena described above, the rotators are equally capable of motion in clockwise and counterclockwise directions. However, true gyroscopic properties are only realized in the limit of unidirectional rotation.<sup>1,17</sup> Although an extended discussion of this subject is beyond the scope of this paper, the most common strategies involve a dipolar rotator, such that rotation can be driven by a rotating electric field of appropriate frequency.<sup>1,58</sup> While complexes  $5^+\text{BF}_4^-$  and  $6^+\text{Z}^-$  fulfill this criterion, they are not ideal in that they are salts, and the counteranion will interact with any rotating dipole, increasing the barrier. Accordingly, in future papers, related neutral complexes will be described that preserve the dipolar rotator.<sup>59</sup>

In summary, this study illustrates the remarkable ease by which iron tricarbonyl based gyroscope-like complexes can be assembled and the quite low rotational barriers that can be achieved in solution and in the solid state without extensive optimization. Subsequent reports will describe systems that have the potential to give still lower barriers through appropriate modifications to both the rotators and stators.

## EXPERIMENTAL SECTION

**General Data.**  $^1\text{H}$ ,  $^{13}\text{C}\{^1\text{H}\}$ , and  $^{31}\text{P}\{^1\text{H}\}$  NMR spectra were recorded on standard 400–500 MHz spectrometers at ambient probe

temperatures unless noted and referenced as follows ( $\delta$ , ppm):  $^1\text{H}$ , residual internal  $\text{C}_6\text{D}_5\text{H}$  (7.15), acetone- $d_5$  (2.05),  $\text{CHCl}_3$  (7.26),  $\text{CDCl}_2\text{H}$  (5.32), or  $\text{CHFCl}_2$  (7.47);  $^{13}\text{C}$ , internal  $\text{C}_6\text{D}_6$  (128.0), acetone- $d_6$  (29.9),  $\text{CDCl}_3$  (77.0),  $\text{CD}_2\text{Cl}_2$  (53.8), or  $\text{CDFCl}_2$  (104.2);  $^{31}\text{P}$ , external  $\text{H}_3\text{PO}_4$  (0.00).  $^{13}\text{C}$  and  $^{31}\text{P}$  solid-state NMR spectra were measured on a Bruker Avance 400 widebore spectrometer equipped with a 2.5 mm multinuclear MAS probehead and  $\text{ZrO}_2$  rotors. For  $^{13}\text{C}$  and  $^{31}\text{P}$  CP/MAS measurements,  $^1\text{H}$  high-power decoupling was applied with contact times of 5 and 2 ms, respectively.  $\text{NH}_4\text{H}_2\text{PO}_4$  was used to establish the  $^{31}\text{P}$  Hartmann–Hahn matching condition and as an external chemical shift standard ( $\delta(^{31}\text{P}) = +0.81$  ppm). For  $^{13}\text{C}$  CP/MAS measurements, adamantane served as Hartmann–Hahn matching and external chemical shift standard ( $\delta(^{13}\text{C}) = 38.52$  ppm). The recycle delay was 3 s for the  $^{13}\text{C}$  and 5 s for the  $^{31}\text{P}$  CP/MAS spectra. Linebroadening factors of 50 Hz were applied for all MAS spectra and 200 Hz for the  $^{31}\text{P}$  wide-line spectrum. The number of transients collected was 64 for the  $^{31}\text{P}$  CP/MAS spectra, 256 for the wide-line spectrum, and 7500 for the  $^{13}\text{C}$  CP/MAS spectrum. The  $^{31}\text{P}$  and  $^{13}\text{C}$  CSA parameters were obtained from the MAS spectra and wide-line spectrum using the program dmfit.<sup>40</sup>

DSC and TGA data were obtained with a Mettler-Toledo DSC-821 instrument.<sup>60</sup> Additional details regarding instrumentation or chemicals are provided in the Supporting Information.

**trans- $\text{Fe}(\text{CO})_3\text{P}((\text{CH}_2)_4\text{CH}=\text{CH}(\text{CH}_2)_3)_2$  (**3a**).** A Schlenk flask was charged with **2a**, trans- $\text{Fe}(\text{CO})_3\text{P}((\text{CH}_2)_4\text{CH}=\text{CH}_2)_2$  (0.262 g, 0.374 mmol),<sup>18a</sup>  $\text{CH}_2\text{Cl}_2$  (50 mL; the resulting solution is 0.0075 M in **2a**), and Grubbs' catalyst (ca. half of 0.040 g, 0.049 mmol, 13 mol %), and fitted with a condenser. The solution was refluxed. After 19 h, the remaining catalyst was added. After another 20 h, the solvent was removed by oil pump vacuum. The residue was filtered through neutral alumina ( $2.5 \times 2.5 \text{ cm}^2$ ) using 2:1 v/v hexane/ $\text{CH}_2\text{Cl}_2$ . The solvent was removed from the filtrate by oil pump vacuum to give *E,E,E*-**3a** as a white solid (0.139 g, 0.226 mmol, 60%), mp 213–216 °C (capillary).<sup>61</sup> TGA: onset of mass loss, 303 °C ( $T_g$ ).<sup>60</sup> Anal. Calcd for  $\text{C}_{33}\text{H}_{34}\text{FeO}_3\text{P}_2$  (616.58): C, 64.31; H, 8.78. Found: C, 64.79; H, 9.00.

**Complex **2a**** (0.198 g, 0.283 mmol),  $\text{CH}_2\text{Cl}_2$  (50 mL; the resulting solution is 0.0057 M in **2a**), and Grubbs' second-generation catalyst (0.026 g, 0.031 mmol, 10 mol %) were similarly combined. The solution was refluxed. After 20 h, the remaining catalyst was added. After another 17 h, the solvent was removed by oil pump vacuum. The residue was filtered through neutral alumina ( $2.5 \times 5.0 \text{ cm}^2$ ) using 2:1 v/v hexane/ $\text{CH}_2\text{Cl}_2$ . The solvent was removed from the filtrate by oil pump vacuum to give *E,E,E*-**3a** as a white solid (0.132 g, 0.214 mmol, 76%). NMR ( $\text{C}_6\text{D}_6$ ,  $\delta$  in ppm):  $^{23}\text{H}$  (400 MHz) 5.49 (m, 6H,  $\text{CH}=\text{}$ ), 2.15 (m, 12H,  $\text{CH}_2\text{CH}=\text{}$ ), 1.79 (m, 12H,  $\text{PCH}_2$ ), 1.49 (m, 24H,  $\text{CH}_2$ );  $^{13}\text{C}\{^1\text{H}\}$  (100 MHz) 213.9 (t,  $^2J_{\text{CP}} = 28.0$  Hz, CO), 132.0 (s,  $\text{CH}=\text{}$ ), 33.4 (s,  $\text{CH}_2\text{CH}=\text{}$ ), 31.0 (virtual t,  $^3J_{\text{CP}}$ ,  $^5J_{\text{CP}} = 7.0$  Hz,  $^2J_{\text{CP}}$   $\text{PCH}_2\text{CH}_2\text{CH}_2$ ), 30.1 (dd,  $^1J_{\text{CP}}$ ,  $^3J_{\text{CP}} = 14.0$ , 12.0 Hz,  $^2J_{\text{CP}}$   $\text{PCH}_2$ ), 24.3 (s,  $\text{PCH}_2\text{CH}_2$ );  $^{31}\text{P}\{^1\text{H}\}$  (162 MHz) 84.7 (s). IR ( $\text{cm}^{-1}$ , powder film) 2926 w, 2849 w, 1853 s ( $\nu_{\text{CO}}$ ), 1436 w, 961 w, 718 w, 645 s. MS:  $^{62}$  616 ( $3a^+$ , 20%), 561 ( $[3a-2\text{CO}]^+$ , 50%), 532 ( $[3a-3\text{CO}]^+$ , 100%).

**trans- $\text{Fe}(\text{CO})_3\text{P}((\text{CH}_2)_5\text{CH}=\text{CH}(\text{CH}_2)_2)_2$  (**3b**).** Complex **2b**, trans- $\text{Fe}(\text{CO})_3\text{P}((\text{CH}_2)_5\text{CH}=\text{CH}_2)_2$  (0.320 g, 0.408 mmol),<sup>18a</sup>  $\text{CH}_2\text{Cl}_2$  (50 mL; the resulting solution is 0.0082 M in **2b**), and Grubbs' catalyst (0.040 g, 0.049 mmol, 12 mol %) were combined in a procedure analogous to that for **3a**. The solution was refluxed. After 20 h, the remaining catalyst was added. After another 24 h, the solvent was removed by oil pump vacuum. The residue was filtered through neutral alumina ( $2.5 \times 4.0 \text{ cm}^2$ ) using 2:1 v/v hexane/ $\text{CH}_2\text{Cl}_2$ . The solvent was removed from the filtrate by oil pump vacuum to give **3b** as a waxy solid (0.208 g, 0.297 mmol, 73%, mixture of *E/Z* isomers). Anal. Calcd for  $\text{C}_{39}\text{H}_{46}\text{FeO}_3\text{P}_2$  (700.75): C, 66.88; H, 9.43. Found: C, 66.96; H, 9.84. NMR ( $\text{C}_6\text{D}_6$ ,  $\delta$  in ppm):  $^1\text{H}$  (400 MHz) 5.69–5.54 (m, 6H,  $\text{CH}=\text{}$ ), 2.33–2.30 (m, 8H,  $\text{CH}_2$ ), 1.79–1.33 (m, 52H,  $\text{CH}_2$ );  $^{31}\text{P}\{^1\text{H}\}$  (162 MHz) 69.8 (s, 44%), 68.5 (s, 39%), 67.4 (s, 13%), 66.1 (s, 4%). IR ( $\text{cm}^{-1}$ , powder film) 3002 w, 2921 m, 2852 m, 1852 s ( $\nu_{\text{CO}}$ ), 1445 m, 1412 m, 1048 w, 1030 w, 969 m, 726 m. MS:  $^{62}$  700 ( $3b^+$ , 50%), 617 ( $[3b-3\text{CO}]^+$ , 100%).



*trans*- $\text{Fe}(\text{CO})_3(\text{P}((\text{CH}_2)_6\text{CH}=\text{CH}(\text{CH}_2)_3)\text{P})$  (**3c**). Complex **2c**, *trans*- $\text{Fe}(\text{CO})_3(\text{P}((\text{CH}_2)_6\text{CH}=\text{CH}_2)_3)_2$  (0.223 g, 0.257 mmol),<sup>18a</sup>  $\text{CH}_2\text{Cl}_2$  (50 mL; the resulting solution is 0.0051 M in **2c**), and Grubbs' catalyst (0.040 g, 0.049 mmol, 19 mol %) were combined in a procedure analogous to that for **3a**. The solution was refluxed. After 18 h, the remaining catalyst was added. After another 20 h, the solvent was removed by oil pump vacuum. The residue was filtered through neutral alumina ( $2.5 \times 2.5 \text{ cm}^2$ ) using 2:1 v/v hexane/ $\text{CH}_2\text{Cl}_2$ . The solvent was removed from the filtrate by oil pump vacuum to give **3c** as a white solid (0.169 g, 0.208 mmol, 81%, mixture of *E/Z* isomers), mp 155–160 °C (capillary). Anal. Calcd for  $\text{C}_{45}\text{H}_{78}\text{FeO}_3\text{P}_2$  (784.91): C, 68.90; H, 9.95. Found: C, 69.24; H, 10.33.

Complex **2c** (0.318 g, 0.366 mmol),  $\text{CH}_2\text{Cl}_2$  (50 mL; the resulting solution is 0.0073 M in **2c**), and Grubbs' second-generation catalyst (0.036 g, 0.0424 mmol, 12 mol %), were similarly combined. The solution was refluxed. After 19 h, the remaining catalyst was added. After another 20 h, the solvent was removed by oil pump vacuum. The residue was filtered through neutral alumina ( $2.5 \times 5.0 \text{ cm}^2$ ) using 2:1 v/v hexane/ $\text{CH}_2\text{Cl}_2$ . The solvent was removed from the filtrate by oil pump vacuum to give **3c** as a white solid (0.226 g, 0.288 mmol, 79%, mixture of *E/Z* isomers). NMR ( $\text{C}_6\text{D}_6$ ,  $\delta$  in ppm):  $^1\text{H}$  (400 MHz) 5.48 (m, 2H,  $\text{CH}=\text{CH}$ ), 5.35 (m, 4H,  $\text{CH}=\text{CH}$ ), 2.06 (m, 12H,  $\text{CH}_2$ ), 1.78–1.69 (m, 20H,  $\text{CH}_2$ ), 1.42 (m, 40H,  $\text{CH}_2$ );  $^{13}\text{C}\{^1\text{H}\}$  (100 MHz) (major isomer only) 215.1 (t,  $^2J_{\text{CP}} = 28.3 \text{ Hz}$ , CO), 131.5 (s,  $\text{CH}=\text{CH}$ ), 32.9 (s,  $\text{CH}_2$ ), 31.9 (virtual t,  $^3J_{\text{CP}}$ ,  $^5J_{\text{CP}} = 6.8 \text{ Hz}$ ,  $^{22}\text{PCH}_2\text{CH}_2\text{CH}_2$ ), 31.6 (dd,  $^1J_{\text{CP}}$ ,  $^3J_{\text{CP}} = 15.2, 12.0 \text{ Hz}$ ,  $^{22}\text{PCH}_2$ ), 29.3 (s,  $\text{CH}_2$ ), 29.2 (s,  $\text{CH}_2$ ), 25.3 (s,  $\text{PCH}_2\text{CH}_2$ );  $^{31}\text{P}\{^1\text{H}\}$  (162 MHz) 71.3 (s, 84%), 70.4 (s, 16%). IR ( $\text{cm}^{-1}$ , powder film) 2926 m, 2853 m, 1930 m, 1861 s ( $\nu_{\text{CO}}$ ), 1459 w, 1440 w, 1409 w, 961 m, 672 m. MS:  $^{62} 784$  ( $3\text{c}^+$ , 10%), 700 ( $[\text{3c-3CO}]^+$ , 100%).

*trans*- $\text{Fe}(\text{CO})_3(\text{P}((\text{CH}_2)_8\text{CH}=\text{CH}(\text{CH}_2)_3)\text{P})$  (**3e**). Complex **2e**, *trans*- $\text{Fe}(\text{CO})_3(\text{P}((\text{CH}_2)_8\text{CH}=\text{CH}_2)_3)_2$  (0.259 g, 0.250 mmol),<sup>18a</sup>  $\text{CH}_2\text{Cl}_2$  (50 mL; the resulting solution is 0.0050 M in **2e**), and Grubbs' catalyst (0.050 g, 0.049 mmol, 24 mol %) were combined in a procedure analogous to that for **3a**. The solution was refluxed. After 18 h, the remaining catalyst was added. After another 21 h, the solvent was removed by oil pump vacuum. A  $^1\text{H}$  NMR spectrum of the residue (0.163 g) showed some residual terminal olefin. Grubbs' catalyst (0.031 g, 0.038 mmol, 15 mol %) and  $\text{CH}_2\text{Cl}_2$  (50 mL) were added and the solution was refluxed. After 20 h, the solvent was removed by oil pump vacuum. The residue was filtered through neutral alumina ( $2.5 \times 4.0 \text{ cm}^2$ ) using 2:1 v/v hexane/ $\text{CH}_2\text{Cl}_2$ . The solvent was removed from the filtrate by oil pump vacuum to give **3e** as a waxy solid (0.149 g, 0.157 mmol, 63%, mixture of *E/Z* isomers). NMR ( $\text{C}_6\text{D}_6$ ,  $\delta$  in ppm):  $^1\text{H}$  (400 MHz) 5.56–5.36 (m, 6H,  $\text{CH}=\text{CH}$ ), 2.08 (m, 10H,  $\text{CH}_2$ ), 1.76 (m, 21H,  $\text{CH}_2$ ), 1.44–1.36 (m, 65H,  $\text{CH}_2$ );  $^{31}\text{P}\{^1\text{H}\}$  (162 MHz) 69.3 (s, 62%), 69.0 (s, 30%), 68.6 (s, 8%).

*trans*- $\text{Fe}(\text{CO})_3(\text{P}((\text{CH}_2)_{10})\text{P})$  (**4a**). A Fischer–Porter bottle was charged with *E,E,E*-**3a** (0.215 g, 0.349 mmol),  $\text{ClRh}(\text{PPh}_3)_3$  (0.050 g, 0.054 mmol, 15 mol %), toluene (10 mL), and  $\text{H}_2$  (5 atm). The solution was stirred at 80 °C. After 48 h, the solvent was removed by oil pump vacuum. The residue was filtered through neutral alumina ( $2.5 \times 5.0 \text{ cm}^2$ ) using 2:1 v/v hexane/ $\text{CH}_2\text{Cl}_2$ . The solvent was removed from the filtrate by oil pump vacuum to give **4a** as a white solid (0.183 g, 0.294 mmol, 84%), mp 165–170 °C (capillary). DSC ( $T_i/T_e/T_p/T_c/T_f$ ): 131.0/150.0/174.3/182.4/185.7 °C (melting endotherm). TGA: onset of mass loss, 346 °C ( $T_e$ ). Anal. Calcd for  $\text{C}_{33}\text{H}_{60}\text{FeO}_3\text{P}_2$  (622.63): C, 63.99; H, 9.65. Found: C, 64.38; H, 9.77. NMR ( $\text{C}_6\text{D}_6$ ,  $\delta$  in ppm):  $^1\text{H}$  (400 MHz) 1.68 (m, 12H,  $\text{PCH}_2$ ), 1.59–1.54 (m, 48H,  $\text{CH}_2$ );  $^{13}\text{C}\{^1\text{H}\}$  (100 MHz) 216.4 (t,  $^2J_{\text{CP}} = 27.5 \text{ Hz}$ , CO), 30.1 (dd,  $^1J_{\text{CP}}$ ,  $^3J_{\text{CP}} = 15.0, 11.7 \text{ Hz}$ ,  $^{22}\text{PCH}_2$ ), 29.1 (virtual t,  $^3J_{\text{CP}}$ ,  $^5J_{\text{CP}} = 5.3 \text{ Hz}$ ,  $^{22}\text{PCH}_2\text{CH}_2\text{CH}_2$ ), 27.5 (s,  $\text{CH}_2$ ), 25.7 (s,  $\text{CH}_2$ ), 21.2 (s,  $\text{PCH}_2\text{CH}_2$ );  $^{31}\text{P}\{^1\text{H}\}$  (162 MHz) 75.5 (s). IR ( $\text{cm}^{-1}$ , powder film) 2922 w, 2853 w, 1841 s ( $\nu_{\text{CO}}$ ), 1455 w, 1413 w, 718 w, 691 w. MS:  $^{62} 622$  ( $4\text{a}^+$ , 50%), 539 ( $[\text{4a-3CO}]^+$ , 100%).

*trans*- $\text{Fe}(\text{CO})_3(\text{P}((\text{CH}_2)_{12})\text{P})$  (**4b**). Complex **3b** (0.246 g, 0.352 mmol),  $\text{ClRh}(\text{PPh}_3)_3$  (0.026 g, 0.028 mmol, 8 mol %), toluene (10 mL), and  $\text{H}_2$  (5 atm) were combined in a procedure analogous to that for **4a**. A similar reaction (70 °C, 68 h) and workup gave **4b** as a white solid (0.214 g, 0.303 mmol, 86%), mp 220–225 °C (capillary). DSC

( $T_i/T_e/T_p/T_c/T_f$ ): 60 –21.2/–1.4/10.1/13.7/20.0 °C (endotherm); 218.7/231.3/250.0/270.0/283.5 °C (melting endotherm). TGA: onset of mass loss, 334 °C ( $T_e$ ). Anal. Calcd for  $\text{C}_{39}\text{H}_{72}\text{FeO}_3\text{P}_2$  (706.79): C, 66.31; H, 10.20. Found: C, 66.22; H, 10.36. NMR ( $\text{C}_6\text{D}_6$ ,  $\delta$  in ppm):  $^1\text{H}$  (400 MHz) 1.80–1.70 (m, 14H,  $\text{CH}_2$ ), 1.65–1.60 (m, 8H,  $\text{CH}_2$ ), 1.48–1.43 (m, 50H,  $\text{CH}_2$ );  $^{13}\text{C}\{^1\text{H}\}$  (100 MHz) 215.5 (t,  $^2J_{\text{CP}} = 28.4 \text{ Hz}$ , CO), 32.0 (dd,  $^1J_{\text{CP}}$ ,  $^3J_{\text{CP}} = 14.7, 12.1 \text{ Hz}$ ,  $^{22}\text{PCH}_2$ ), 29.9 (virtual t,  $^3J_{\text{CP}}$ ,  $^5J_{\text{CP}} = 7.2 \text{ Hz}$ ,  $^{22}\text{PCH}_2\text{CH}_2\text{CH}_2$ ), 27.8 (s,  $\text{CH}_2$ ), 27.5 (s,  $\text{CH}_2$ ), 26.3 (s,  $\text{CH}_2$ ), 22.9 (s,  $\text{PCH}_2\text{CH}_2$ );  $^{31}\text{P}\{^1\text{H}\}$  (162 MHz) 67.5 (s). IR ( $\text{cm}^{-1}$ , powder film) 2926 m, 2853 m, 1853 s ( $\nu_{\text{CO}}$ ), 1459 w, 1413 w, 803 w, 741 w, 641 s. MS:  $^{62} 706$  ( $4\text{b}^+$ , 20%), 622 ( $[\text{4b-3CO}]^+$ , 100%).

*trans*- $\text{Fe}(\text{CO})_3(\text{P}((\text{CH}_2)_{14})\text{P})$  (**4c**). Complex **3c** (0.164 g, 0.209 mmol),  $\text{ClRh}(\text{PPh}_3)_3$  (0.025 g, 0.027 mmol, 13 mol %), toluene (10 mL), and  $\text{H}_2$  (5 atm) were combined in a procedure analogous to that for **4a**. A similar reaction (60 °C, 72 h) and workup gave **4c** as a white solid (0.130 g, 0.165 mmol, 79%), mp 163–168 °C (capillary). DSC ( $T_i/T_e/T_p/T_c/T_f$ ): 128.2/157.9/173.6/177.2/181.8 °C (melting endotherm; no other phase transitions, –100 to 150 °C). TGA: onset of mass loss, 341 °C ( $T_e$ ). Anal. Calcd for  $\text{C}_{45}\text{H}_{84}\text{FeO}_3\text{P}_2$  (790.96): C, 68.33; H, 10.71. Found: C, 68.05; H, 10.90. NMR ( $\text{C}_6\text{D}_6$ ,  $\delta$  in ppm):  $^1\text{H}$  (400 MHz) 1.75 (m, 24H,  $\text{PCH}_2$  and  $\text{PCH}_2\text{CH}_2$ ), 1.45–1.41 (m, 60H,  $\text{CH}_2$ );  $^{13}\text{C}\{^1\text{H}\}$  (100 MHz) 215.6 (t,  $^2J_{\text{CP}} = 29.0 \text{ Hz}$ , CO), 31.6 (dd,  $^1J_{\text{CP}}$ ,  $^3J_{\text{CP}} = 15.1, 11.7 \text{ Hz}$ ,  $^{22}\text{PCH}_2$ ), 31.0 (virtual t,  $^3J_{\text{CP}}$ ,  $^5J_{\text{CP}} = 6.6 \text{ Hz}$ ,  $^{22}\text{PCH}_2\text{PCH}_2\text{CH}_2$ ), 28.2 (s,  $\text{CH}_2$ ), 28.0 (s,  $\text{CH}_2$ ), 27.1 (s,  $\text{CH}_2$ ), 26.5 (s,  $\text{CH}_2$ ), 24.0 (s,  $\text{PCH}_2\text{CH}_2$ );  $^{31}\text{P}\{^1\text{H}\}$  (162 MHz) 66.9 (s). IR ( $\text{cm}^{-1}$ , powder film) 2926 m, 2856 m, 1861 s ( $\nu_{\text{CO}}$ ), 1459 w, 737 w, 645 m. MS:  $^{62} 790$  ( $4\text{c}^+$ , 20%), 736 ( $[\text{4c-2CO}]^+$ , 30%), 706 ( $[\text{4c-3CO}]^+$ , 100%).

*trans*- $\text{Fe}(\text{CO})_3(\text{P}((\text{CH}_2)_{18})\text{P})$  (**4e**). Complex **3e** (0.149 g, 0.157 mmol),  $\text{ClRh}(\text{PPh}_3)_3$  (0.096 g, 0.103 mmol, 10 mol %), toluene (10 mL), and  $\text{H}_2$  (5 atm) were combined in a procedure analogous to that for **4a**. A similar reaction (65 °C, 72 h), alumina filtration ( $2.5 \times 5.0 \text{ cm}^2$ , 3:1 v/v hexane/ $\text{CH}_2\text{Cl}_2$ ), and workup gave **4e** as a colorless oil, which became a waxy solid after an additional week (0.738 g, 0.770 mmol, 74%). Anal. Calcd for  $\text{C}_{57}\text{H}_{108}\text{FeO}_3\text{P}_2$  (875.12): C, 71.37; H, 11.37. Found: C, 71.95; H, 10.94.<sup>63</sup> NMR ( $\text{C}_6\text{D}_6$ ,  $\delta$  in ppm):  $^1\text{H}$  (400 MHz) 1.76 (m, 24H,  $\text{PCH}_2$  and  $\text{PCH}_2\text{CH}_2$ ), 1.41–1.34 (m, 84H,  $\text{CH}_2$ );  $^{13}\text{C}\{^1\text{H}\}$  (100 MHz) 215.7 (t,  $^2J_{\text{CP}} = 28.0 \text{ Hz}$ , CO), 31.6 (virtual t,  $^3J_{\text{CP}}$ ,  $^5J_{\text{CP}} = 6.1 \text{ Hz}$ ,  $^{22}\text{PCH}_2\text{CH}_2\text{CH}_2$ ), 31.2 (dd,  $^1J_{\text{CP}}$ ,  $^3J_{\text{CP}} = 14.9, 12.1 \text{ Hz}$ ,  $^{22}\text{PCH}_2$ ), 29.4 (s,  $\text{CH}_2$ ), 29.2 (s,  $\text{CH}_2$ ), 28.8 (s,  $\text{CH}_2$ ), 28.3 (s,  $\text{CH}_2$ ), 28.1 (s,  $\text{CH}_2$ ), 27.5 (s,  $\text{CH}_2$ ), 24.3 (s,  $\text{PCH}_2\text{CH}_2$ );  $^{31}\text{P}\{^1\text{H}\}$  (162 MHz) 66.0 (s). IR ( $\text{cm}^{-1}$ , oil film) 2922 m, 2850 m, 1859 s ( $\nu_{\text{CO}}$ ), 1460 w, 740 w, 642 m.

$[\text{trans-Fe}(\text{CO})_2(\text{NO})(\text{P}((\text{CH}_2)_{10})\text{P})]^+\text{BF}_4^-$  (**5a** $^+\text{BF}_4^-$ ). A Schlenk flask was charged with **4a** (0.123 g, 0.198 mmol) and  $\text{CH}_2\text{Cl}_2$  (8 mL). Then  $\text{NO}^+\text{BF}_4^-$  (0.0325 g, 0.278 mmol) was added with stirring. After 15 h, the solvent was removed by oil pump vacuum. The residue was extracted with acetone, and the extract was filtered through a Celite plug over sintered glass. The solvent was removed by oil pump vacuum, and the residue was triturated under ether. The ether was decanted and the residue dried by oil pump vacuum to give **5a** $^+\text{BF}_4^-$  as a yellow solid (0.138 g, 0.194 mmol, 98%), mp 206–208 °C (capillary). Anal. Calcd for  $\text{C}_{32}\text{H}_{60}\text{BF}_4\text{FeNO}_3\text{P}_2$  (711.43): C, 54.04; H, 8.44; N, 1.97. Found: C, 52.39; H, 8.71; N, 1.85.<sup>63</sup> NMR ( $\text{CDCl}_3$ ,  $\delta$  in ppm):  $^1\text{H}$  (400 MHz) 2.27–2.10 (m, 12H,  $\text{PCH}_2$ ), 1.65–1.58 (m, 18H,  $\text{CH}_2$ ), 1.47–1.27 (m, 30H,  $\text{CH}_2$ );  $^{13}\text{C}\{^1\text{H}\}$  (100 MHz) 208.7 (t,  $^2J_{\text{CP}} = 25.1 \text{ Hz}$ , CO), 28.3 (virtual t,  $^3J_{\text{CP}}$ ,  $^5J_{\text{CP}} = 5.3 \text{ Hz}$ ,  $^{22}\text{2PCH}_2\text{CH}_2\text{CH}_2$ ), 27.9–27.6 (overlapping virtual t/m,  $1\text{PCH}_2\text{CH}_2\text{CH}_2$ ,  $2\text{PCH}_2$ ,  $1\text{PCH}_2$ ), 26.8 and 26.7 (2s,  $1\text{CH}_2$  and  $2\text{CH}_2$ ), 25.0 and 24.2 (2s,  $2\text{CH}_2$  and  $1\text{CH}_2$ ), 22.3 and 21.4 (2s,  $1\text{PCH}_2\text{CH}_2$  and  $2\text{PCH}_2\text{CH}_2$ );  $^{31}\text{P}\{^1\text{H}\}$  (162 MHz) 67.0 (s). IR ( $\text{cm}^{-1}$ , powder film) 2926 m, 2856 w, 2023 m ( $\nu_{\text{CO}}$ ), 1953 s ( $\nu_{\text{CO}}$ ), 1752 s ( $\nu_{\text{NO}}$ ), 1459 w, 1413 w, 1046 s, 714 m, 637 s. MS:  $^{62} 625$  ( $5\text{a}^+$ , 50%), 597 ( $[\text{5a-CO}]^+$ , 20%), 569 ( $[\text{5a-2CO}]^+$ , 100%).

$[\text{trans-Fe}(\text{CO})_2(\text{NO})(\text{P}((\text{CH}_2)_{12})\text{P})]^+\text{BF}_4^-$  (**5b** $^+\text{BF}_4^-$ ). Complex **4b** (0.0840 g, 0.119 mmol),  $\text{CH}_2\text{Cl}_2$  (5 mL), and  $\text{NO}^+\text{BF}_4^-$  (0.0230 g, 0.197 mmol) were combined in a procedure analogous to that for **5a** $^+\text{BF}_4^-$ . An identical workup gave **5b** $^+\text{BF}_4^-$  as a yellow solid (0.0845 g,

0.106 mmol, 89%), mp 204–206 °C (capillary). Anal. Calcd for  $C_{38}H_{72}BF_4FeNO_3P_2$  (795.59): C, 57.39; H, 9.06; N, 1.76. Found: C, 57.43; H, 9.43; N, 1.50. NMR ( $CDCl_3$ ,  $\delta$  in ppm):  $^{23}H$  (400 MHz) 2.26 (m, 12H,  $PCH_2$ ), 1.57 (m, 20H,  $CH_2$ ), 1.41–1.28 (m, 40H,  $CH_2$ );  $^{13}C\{^1H\}$  (100 MHz) 207.5 (t,  $^2J_{CP} = 24.8$  Hz, CO), 29.5–28.6 (overlapping virtual t/m,  $2PCH_2CH_2CH_2$ ,  $1PCH_2CH_2CH_2$ ,  $2PCH_2$ , and  $1PCH_2$ ), 27.1 and 27.0 (2s,  $2CH_2$  and  $1CH_2$ ), 26.8 and 26.6 (2s,  $2CH_2$  and  $1CH_2$ ), 25.8 and 25.7 (2s,  $2CH_2$  and  $1CH_2$ ), 23.2 and 23.0 (2s,  $1PCH_2CH_2$  and  $2PCH_2CH_2$ );  $^{31}P\{^1H\}$  (162 MHz) 57.5 (s). IR ( $cm^{-1}$ , powder film) 2926 m, 2856 w, 2026 m ( $\nu_{CO}$ ), 1965 s ( $\nu_{CO}$ ), 1764 s ( $\nu_{NO}$ ), 1459 w, 1413 w, 1046 s, 633 m. MS:  $^{62}708$  ( $5b^+$ , 50%), 652 ( $[5b-2CO]^+$ , 100%).

**[trans-Fe(CO)<sub>2</sub>(NO)(P((CH<sub>2</sub>)<sub>14</sub>3P)]<sup>+</sup>BF<sub>4</sub><sup>−</sup> (**5c**<sup>+</sup>BF<sub>4</sub><sup>−</sup>).** Complex **4c** (0.0730 g, 0.0924 mmol),  $CH_2Cl_2$  (5 mL), and  $NO^+BF_4^-$  (0.0190 g, 0.163 mmol) were combined in a procedure analogous to that for **5a**<sup>+</sup>BF<sub>4</sub><sup>−</sup>. An identical workup gave **5c**<sup>+</sup>BF<sub>4</sub><sup>−</sup> as a yellow solid (0.0657 g, 0.0748 mmol, 81%), mp 168–170 °C (capillary). Anal. Calcd for  $C_{44}H_{84}BF_4FeNO_3P_2$  (879.76): C, 60.10; H, 9.56; N, 1.59. Found: C, 58.64; H, 9.51; N, 1.53.  $^{63}NMR$  (acetone-*d*<sub>6</sub>,  $\delta$  in ppm):  $^{23}H$  (400 MHz) 2.42 (m, 12H,  $PCH_2$ ), 1.66–1.56 (m, 24H,  $PCH_2CH_2$  and  $PCH_2CH_2CH_2$ ), 1.36–1.31 (m, 48H,  $CH_2$ );  $^{13}C\{^1H\}$  (100 MHz) 208.2 (t,  $^2J_{CP} = 25.3$  Hz, CO), 30.7 (virtual t,  $^3J_{CP}$ ,  $^5J_{CP} = 7.6$  Hz,  $^{22}PCH_2CH_2CH_2$ ), 28.7 (dd,  $^1J_{CP}$ ,  $^3J_{CP} = 15.4$ , 13.5 Hz,  $PCH_2$ ), 28.2 (s,  $CH_2$ ), 28.0 (s,  $CH_2$ ), 27.2 (s,  $CH_2$ ), 26.6 (s,  $CH_2$ ), 24.6 (s,  $PCH_2CH_2$ );  $^{31}P\{^1H\}$  (162 MHz) 56.8 (s). IR ( $cm^{-1}$ , powder film) 2926 m, 2856 m, 2030 m ( $\nu_{CO}$ ), 1965 s ( $\nu_{CO}$ ), 1764 s ( $\nu_{NO}$ ), 1459 w, 1413 w, 1054 s, 726 m, 633 s. MS:  $^{62}793$  (**5c**<sup>+</sup>, 30%), 737 ( $[5c-2CO]^+$ , 100%).

**mer,trans-[Fe(CO)<sub>3</sub>(H)(P((CH<sub>2</sub>)<sub>10</sub>3P)]<sup>+</sup>BARf<sup>−</sup> (**6a**<sup>+</sup>BARf<sup>−</sup>).** A Schlenk flask was charged with **4a** (0.0250 g, 0.0402 mmol),  $CH_2Cl_2$  (8.0 mL), and  $[H(OEt_2)_2]^+BARf^-$  (0.041 g, 0.040 mmol) with stirring. After 24 h, the solvent was removed by oil pump vacuum. The residue was washed with hexane and dried by oil pump vacuum to give **6a**<sup>+</sup>BARf<sup>−</sup> as an off-white powder (0.059 g, 0.040 mmol, 99%), mp 162–167 °C (capillary; greenish liquid). Anal. Calcd for  $C_{65}H_{73}BF_4FeO_3P_2$  (1486.86): C, 52.51; H, 4.95. Found: C, 52.37; H, 5.04. NMR ( $CD_2Cl_2$ ,  $\delta$  in ppm):  $^1H$  (500 MHz) 7.74–7.70 (m, 8H,  $C_6H_3$  o to B), 7.58–7.53 (m, 4H,  $C_6H_3$  p to B), 2.05–1.81 (m, 12H,  $CH_2$ ), 1.70–1.22 (m, 48H,  $CH_2$ ), −9.44 (t,  $^2J_{PH} = 22.17$  Hz, 1H, FeH);  $^{13}C\{^1H\}$  (125 MHz) 206.8 (t,  $^2J_{CP} = 20.7$  Hz, CO *trans* to H), 206.0 (t,  $^2J_{CP} = 20.7$  Hz, CO *cis* to H), 162.2 (q,  $^1J_{BC} = 50$  Hz,  $C_6H_3$  i to B), 135.3 (s,  $C_6H_3$  ortho to B), 129.3 (q,  $^2J_{CF} = 31$  Hz,  $C_6H_3$  m to B), 123.6 (q,  $^1J_{CF} = 272$  Hz, CF<sub>3</sub>), 117.9 (s,  $C_6H_3$  p to B), 28.7 (dd,  $^1J_{CP}$ ,  $^3J_{CP} = 15.1$  Hz, 15.0 Hz,  $^{22}2PCH_2$ ) and 28.0 (dd,  $^1J_{CP}$ ,  $^3J_{CP} = 15.1$  Hz, 15.0 Hz,  $^{22}1PCH_2$ ), 28.6–28.4 (overlapping virtual t,  $^3J_{CP}$ ,  $^5J_{CP} = 5.8$  Hz,  $^{22}PCH_2CH_2CH_2$ ), 26.8 and 26.5 (2s,  $2CH_2$  and  $1CH_2$ ), 26.2 and 25.4 (2s,  $1CH_2$  and  $2CH_2$ ), 22.1 and 20.5 (2s,  $1PCH_2CH_2$  and  $2PCH_2CH_2$ );  $^{31}P\{^1H\}$  (202 MHz) 59.7 (s). IR ( $cm^{-1}$ , powder film) 2933 w, 2860 w, 2059 w ( $\nu_{CO}$ ), 2007 m ( $\nu_{CO}$ ), 1992 s ( $\nu_{CO}$ ), 1608 w, 1458 w, 1352 s, 1273 s.

**mer,trans-[Fe(CO)<sub>3</sub>(H)(P((CH<sub>2</sub>)<sub>12</sub>3P)]<sup>+</sup>BARf<sup>−</sup> (**6b**<sup>+</sup>BARf<sup>−</sup>).** Complex **4b** (0.0250 g, 0.0354 mmol),  $CH_2Cl_2$  (8.0 mL), and  $[H(OEt_2)_2]^+BARf^-$  (0.036 g, 0.035 mmol) were combined in a procedure analogous to that for **6a**<sup>+</sup>BARf<sup>−</sup>. An identical workup gave **6b**<sup>+</sup>BARf<sup>−</sup> as an off-white powder (0.055 g, 0.035 mmol, 99%), mp 161–165 °C (capillary; greenish liquid). Anal. Calcd for  $C_{71}H_{85}BF_4FeO_3P_2$  (1571.02): C, 54.28; H, 5.45. Found: C, 54.15; H, 5.46. NMR ( $CD_2Cl_2$ ,  $\delta$  in ppm):  $^1H$  (500 MHz) 7.75–7.69 (m, 8H,  $C_6H_3$  ortho to B), 7.58–7.54 (m, 4H,  $C_6H_3$  p to B), 1.99–1.87 (m, 12H,  $CH_2$ ), 1.60–1.49 (m, 24H,  $CH_2$ ), 1.47–1.40 (m, 12H,  $CH_2$ ), 1.38–1.29 (m, 24H,  $CH_2$ ), −9.45 (t,  $^2J_{PH} = 27.1$  Hz, 1H, FeH);  $^{13}C\{^1H\}$  (125 MHz) 206.8–206.2 (overlapping triplets, CO), 162.2 (q,  $^1J_{BC} = 50$  Hz,  $C_6H_3$  i to B), 135.2 (s,  $C_6H_3$  ortho to B), 129.3 (q,  $^2J_{CF} = 31$  Hz,  $C_6H_3$  m to B), 123.6 (q,  $^1J_{CF} = 272$  Hz, CF<sub>3</sub>), 117.9 (s,  $C_6H_3$  p to B), 30.8 (virtual t,  $^3J_{CP}$ ,  $^5J_{CP} = 15.4$  Hz,  $^{22}PCH_2$ ), 29.2 (virtual t,  $^3J_{CP}$ ,  $^5J_{CP} = 7.2$  Hz,  $^{22}PCH_2CH_2CH_2$ ), 27.5 (s,  $CH_2$ ), 27.2 (s,  $CH_2$ ), 26.7 (s,  $CH_2$ ), 23.2 (s,  $PCH_2CH_2$ );  $^{31}P\{^1H\}$  (202 MHz) 49.9 (s). IR ( $cm^{-1}$ , powder film) 2931 w, 2860 w, 2073 w ( $\nu_{CO}$ ), 2025 m ( $\nu_{CO}$ ), 1998 s ( $\nu_{CO}$ ), 1610 w, 1458 w, 1352 s, 1275 s, 1157 s, 1120 s, 887 m, 713 s, 680 m, 669 m.

**mer,trans-[Fe(CO)<sub>3</sub>(H)(P((CH<sub>2</sub>)<sub>14</sub>3P)]<sup>+</sup>BARf<sup>−</sup> (**6c**<sup>+</sup>BARf<sup>−</sup>).** Complex **4c** (0.0250 g, 0.0316 mmol),  $CH_2Cl_2$  (8.0 mL), and  $[H(OEt_2)_2]^+BARf^-$

(0.032 g, 0.032 mmol) were combined in a procedure analogous to that for **6a**<sup>+</sup>BARf<sup>−</sup>. An identical workup gave **6c**<sup>+</sup>BARf<sup>−</sup> as an off-white powder (0.051 g, 0.031 mmol, 98%), mp 185–188 °C (capillary; greenish liquid). Anal. Calcd for  $C_{77}H_{97}BF_4FeO_3P_2$  (1655.18): C, 55.91; H, 5.85. Found: C, 55.26; H, 5.76.  $^{63}NMR$  ( $CD_2Cl_2$ ,  $\delta$  in ppm):  $^{23}H$  (500 MHz) 7.75–7.70 (m, 8H,  $C_6H_3$  o to B), 7.60–7.55 (m, 4H,  $C_6H_3$  p to B), 2.00–1.88 (m, 12H,  $CH_2$ ), 1.60–1.45 (m, 24H,  $CH_2$ ), 1.44–1.24 (m, 48H,  $CH_2$ ), −9.45 (t,  $^2J_{PH} = 30.2$  Hz, 1H, FeH);  $^{13}C\{^1H\}$  (125 MHz) 206.8 (t,  $^2J_{CP} = 21.1$  Hz, CO *cis* to H), 206.0 (t,  $^2J_{CP} = 15.0$  Hz, CO *trans* to H), 162.2 (q,  $^1J_{BC} = 50$  Hz,  $C_6H_3$  i to B), 135.3 (s,  $C_6H_3$  o to B), 129.3 (q,  $^2J_{CF} = 31$  Hz,  $C_6H_3$  m to B), 125.4 (q,  $^1J_{CF} = 272$  Hz, CF<sub>3</sub>), 117.9 (s,  $C_6H_3$  p to B), 30.13 (virtual t,  $^3J_{CP}$ ,  $^5J_{CP} = 15.1$  Hz,  $^{22}PCH_2$ ), 30.08 (overlapping virtual t,  $^3J_{CP}$ ,  $^5J_{CP} = 5.5$  Hz,  $^{22}PCH_2CH_2CH_2$ ), 27.9 (s,  $CH_2$ ), 27.7 (s,  $CH_2$ ), 27.28 (s,  $CH_2$ ), 27.26 (s,  $CH_2$ ), 23.9 (s,  $PCH_2CH_2$ );  $^{31}P\{^1H\}$  (202 MHz) 46.9 (s). IR ( $cm^{-1}$ , powder film) 2931 w, 2858 w, 2081 w ( $\nu_{CO}$ ), 2031 m ( $\nu_{CO}$ ), 2015 s ( $\nu_{CO}$ ), 1608 w, 1352 s, 1276 s.

**mer,trans-[Fe(CO)<sub>3</sub>(H)(P((CH<sub>2</sub>)<sub>18</sub>3P)]<sup>+</sup>BARf<sup>−</sup> (**6e**<sup>+</sup>BARf<sup>−</sup>).** Complex **4e** (0.0250 g, 0.0261 mmol),  $CH_2Cl_2$  (8.0 mL), and  $[H(OEt_2)_2]^+BARf^-$  (0.026 g, 0.026 mmol) were combined in a procedure analogous to that for **6a**<sup>+</sup>BARf<sup>−</sup>. An identical workup gave **6e**<sup>+</sup>BARf<sup>−</sup> as a yellow gum (0.046 g, 0.026 mmol, 99%). Anal. Calcd for  $C_{89}H_{121}BF_4FeO_3P_2$  (1823.51): C, 58.62; H, 6.69. Found: C, 59.26; H, 6.83.  $^{63}NMR$  ( $CD_2Cl_2$ ,  $\delta$  in ppm):  $^{23}H$  (500 MHz) 7.76–7.72 (m, 8H,  $C_6H_3$  o to B), 7.59–7.57 (m, 4H,  $C_6H_3$  p to B), 2.01–1.89 (m, 12H,  $CH_2$ ), 1.61–1.45 (m, 24H,  $CH_2$ ), 1.43–1.24 (m, 72H,  $CH_2$ ), −9.48 (t,  $^2J_{PH} = 32.2$  Hz, 1H, FeH);  $^{13}C\{^1H\}$  (125 MHz) 207.0 (t,  $^2J_{CP} = 22.1$  Hz, CO *cis* to H), 206.0 (t,  $^2J_{CP} = 13.6$  Hz, CO *trans* to H), 162.2 (q,  $^1J_{BC} = 55$  Hz,  $C_6H_3$  i to B), 135.3 (s,  $C_6H_3$  o to B), 129.4 (q,  $^2J_{CF} = 33$  Hz,  $C_6H_3$  m to B), 125.1 (q,  $^1J_{CF} = 273$  Hz, CF<sub>3</sub>), 117.9 (s,  $C_6H_3$  p to B), 30.7 (virtual t,  $^3J_{CP}$ ,  $^5J_{CP} = 6.9$  Hz,  $^{22}PCH_2CH_2CH_2$ ), 29.3 (virtual t,  $^3J_{CP}$ ,  $^5J_{CP} = 14.7$  Hz,  $^{22}PCH_2$ ), 28.8 (s,  $CH_2$ ), 28.7 (s,  $CH_2$ ), 28.6 (s,  $CH_2$ ), 28.56 (s,  $CH_2$ ), 28.3 (s,  $CH_2$ ), 28.2 (s,  $CH_2$ ), 23.9 (s,  $PCH_2CH_2$ );  $^{31}P\{^1H\}$  (202 MHz) 43.4 (s). IR ( $cm^{-1}$ , oil film) 2927 w, 2856 w, 2081 w ( $\nu_{CO}$ ), 2025 m ( $\nu_{CO}$ ), 2009 s ( $\nu_{CO}$ ), 1608 w, 1440 w, 1352 s, 1273 s.

**mer,trans-[Fe(CO)<sub>3</sub>(H)(P((CH<sub>2</sub>)<sub>4</sub>CH=CH(CH<sub>2</sub>)<sub>4</sub>)<sub>3</sub>P)]<sup>+</sup>BARf<sup>−</sup> (**7a**<sup>+</sup>BARf<sup>−</sup>).** Complex **E,E,E-3a** (0.0250 g, 0.0405 mmol),  $CH_2Cl_2$  (8.0 mL), and  $[H(OEt_2)_2]^+BARf^-$  (0.041 g, 0.041 mmol) were combined in a procedure analogous to that for **6a**<sup>+</sup>BARf<sup>−</sup>. An identical workup gave **E,E,E-7a**<sup>+</sup>BARf<sup>−</sup> as an off-white powder (0.058 g, 0.039 mmol, 97%), mp 156–158 °C (capillary; greenish liquid). Anal. Calcd for  $C_{65}H_{67}BF_4FeO_3P_2$  (1480.81): C, 52.76; H, 4.50. Found: C, 52.96; H, 4.78. NMR ( $CD_2Cl_2$ ,  $\delta$  in ppm):  $^1H$  (500 MHz) 7.77–7.71 (m, 8H,  $C_6H_3$  o to B), 7.60–7.57 (m, 4H,  $C_6H_3$  p to B), 5.48–5.44 (m, 2H,  $CH=CH$ ), 5.33–5.30 (m, 4H,  $CH=CH$ ), 2.17–2.07 (m, 12H,  $CH_2$ ), 2.00–1.79 (m, 12H,  $CH_2$ ), 1.72–1.45 (m, 30H,  $CH_2$ ), −9.40 (t,  $^2J_{PH} = 22.1$  Hz, 1H, FeH);  $^{13}C\{^1H\}$  (125 MHz) 206.3–205.8 (overlapping triplets, CO), 162.1 (q,  $^1J_{BC} = 50$  Hz,  $C_6H_3$  i to B), 135.2 (s,  $C_6H_3$  o to B), 132.6 (s, 2  $CH_2=$ ), 131.9 (s, 1  $CH_2=$ ), 129.2 (q,  $^2J_{CF} = 31$  Hz,  $C_6H_3$  m to B), 125.0 (q,  $^1J_{CF} = 272$  Hz, CF<sub>3</sub>), 117.9 (s,  $C_6H_3$  p to B), 33.1 (s, 2  $CH_2CH=$ ), 31.2 (s, 1  $CH_2CH=$ ), 30.0 (virtual t,  $^3J_{CP}$ ,  $^5J_{CP} = 7.6$  Hz,  $^{22}2PCH_2CH_2CH_2$ ), 29.7 (virtual t,  $^3J_{CP}$ ,  $^5J_{CP} = 5.2$  Hz,  $^{22}1PCH_2CH_2CH_2$ ), 29.1 (dd,  $^1J_{CP}$ ,  $^3J_{CP} = 15.7$ , 14.5 Hz,  $^{22}2PCH_2$ ), 27.3 (dd,  $^1J_{CP}$ ,  $^3J_{CP} = 15.3$ , 14.1 Hz,  $^{22}1PCH_2$ ), 25.6 (s,  $2PCH_2CH_2$ ), 22.5 (s,  $1PCH_2CH_2$ );  $^{31}P\{^1H\}$  (202 MHz) 66.4 (s). IR ( $cm^{-1}$ , powder film) 2933 w, 2858 w, 2067 w ( $\nu_{CO}$ ), 2015 m ( $\nu_{CO}$ ), 2000 s ( $\nu_{CO}$ ), 1610 w, 1440 w, 1352 s, 1273 s.

**Cyclic Voltammetry.** A BASiEpsilon Electrochemical Workstation (Cell Stand C3) with the program Epsilon EC (version 2.13.77) was employed. Samples were prepared under  $N_2$ , and data were recorded as described in Table 2 (ferrocene added after each measurement).

**Crystallography.** Complex **4c** was suspended in methanol and warmed. THF was added until the sample was homogeneous. After 1 day at room temperature, colorless prisms were obtained. Data were collected as outlined in Table S1. Cell parameters were obtained from 10 frames using a  $10^\circ$  scan and refined with 10223 reflections. Lorentz, polarization, and absorption corrections were applied.<sup>64</sup> The space group was determined from systematic absences and subsequent least-squares refinement. The structure was solved by direct methods. The parameters were refined with all data by full-matrix-least-squares



on  $F^2$  using SHELXL-97.<sup>65</sup> Non-hydrogen atoms were refined with anisotropic thermal parameters. The hydrogen atoms were fixed in idealized positions using a riding model. Scattering factors were taken from literature.<sup>66</sup>

A solution of  $E,E,E$ -3a in hexane/benzene (2 mL, 1:1 v/v) was kept in a freezer ( $-20^\circ\text{C}$ ). After 1 day, a colorless prism was obtained, which upon warming to room temperature turned white. Data were collected as outlined in Table S1. Cell parameters were obtained from 10 images using a  $10^\circ$  scan and refined with 3060 reflections. Using Olex2,<sup>67</sup> the structure was solved with SHELXS<sup>65</sup> by direct methods and refined with SHELXL<sup>65</sup> using least-squares minimization. The space group was determined by systematic absences and intensity statistics. Non-hydrogen atoms were refined with anisotropic thermal parameters. The hydrogen atoms were fixed in idealized position using a riding model. Scattering factors were taken from literature.<sup>66</sup>

A white prism of  $E,E,E$ -3a·2(1,3,5- $\text{C}_6\text{H}_3(\text{CH}_3)_3$ ) was analogously obtained from  $E,E,E$ -3a (0.150 g) using hexane/mesitylene. The structure was solved by an identical series of procedures (cell parameters from 10 images using a  $10^\circ$  scan and refined with 8529 reflections).

## ■ ASSOCIATED CONTENT

### ■ Supporting Information

The Supporting Information is available free of charge on the ACS Publications website at DOI: 10.1021/jacs.6b03178.

Additional experimental procedures, crystallographic data, and Eyring plots (PDF)

Crystallographic information file for compounds  $E,E,E$ -3a· $\text{C}_6\text{H}_6$ ,  $E,E,E$ -3a·2(1,3,5- $\text{C}_6\text{H}_3(\text{CH}_3)_3$ ), and 4c (CIF)

## ■ AUTHOR INFORMATION

### Corresponding Author

\*E-mail: gladysz@mail.chem.tamu.edu.

### Notes

The authors declare no competing financial interest.

## ■ ACKNOWLEDGMENTS

We thank the US National Science Foundation (CHE-1300208, J.B.; CHE-0719267 and CHE-1153085, J.A.G.) and Deutsche Forschungsgemeinschaft (DFG, GL 300/9-1) for support, Dr. Vladimir Bakhmutov for recording the variable temperature solid-state NMR spectra, and Ms. Yanyan Wang for assistance with some DSC measurements.

## ■ REFERENCES

- (1) Kottas, G. S.; Clarke, L. I.; Horinek, D.; Michl, J. *Chem. Rev.* **2005**, *105*, 1281–1376.
- (2) (a) Guix, M.; Mayorga-Martinez, C. C.; Merkoçi, A. *Chem. Rev.* **2014**, *114*, 6285–6322. (b) Abendroth, J. M.; Bushuyev, O. S.; Weiss, P. S.; Barrett, C. J. *ACS Nano* **2015**, *9*, 7746–7768.
- (3) (a) Vives, G.; Tour, J. M. *Acc. Chem. Res.* **2009**, *42*, 473–487. (b) García-López, V.; Chu, P.-L. E.; Chiang, P.-T.; Sun, J.; Martí, A. A.; Tour, J. M. *Asian J. Org. Chem.* **2015**, *4*, 1308–1314 and earlier work cited therein.
- (4) Various representative examples: (a) Lemouchi, C.; Iliopoulos, K.; Zorina, L.; Simonov, S.; Wzietek, P.; Cauchy, T.; Rodríguez-Fortea, A.; Canadell, E.; Kaleta, J.; Michl, J.; Gindre, D.; Chrysos, M.; Batail, P. J. *Am. Chem. Soc.* **2013**, *135*, 9366–9376. (b) Zhou, Z.; Zhang, X.; Liu, Q.; Yan, Z.; Lv, C.; Long, G. *Inorg. Chem.* **2013**, *52*, 10258–10263. (c) Liu, Z.-q.; Kubo, K.; Noro, S.-i.; Akutagawa, T.; Nakamura, T. *Cryst. Growth Des.* **2014**, *14*, 537–543, and earlier work cited therein. (d) Chen, J.; Kistemaker, J. C. M.; Robertus, J.; Feringa, B. L. *J. Am. Chem. Soc.* **2014**, *136*, 14924–14932. (e) Zigon, N.; Hosseini, M. W. *Chem. Commun.* **2015**, *51*, 12486–12489, and earlier work cited therein. (f) Prack, E.; O'Keefe, C. A.; Moore, J. K.; Lai, A.; Lough, A. J.; Macdonald, P. M.; Conradi, M. S.; Schurko, R. W.; Fekl, U. *J. Am. Chem. Soc.* **2015**, *137*, 13464–13467.

- (5) (a) Khuong, T.-A. V.; Nuñez, J. E.; Godinez, C. E.; Garcia-Garibay, M. A. *Acc. Chem. Res.* **2006**, *39*, 413–422. (b) Vogelsberg, C. S.; Garcia-Garibay, M. A. *Chem. Soc. Rev.* **2012**, *41*, 1892–1910. (c) Pérez-Estrada, S.; Rodríguez-Molina, B.; Xiao, L.; Santillan, R.; Jiménez-Osés, G.; Houk, K. N.; Garcia-Garibay, M. A. *J. Am. Chem. Soc.* **2015**, *137*, 2175–2178. (d) Arcos-Ramos, R.; Rodríguez-Molina, B.; Gonzalez-Rodriguez, E.; Ramirez-Montes, P. I.; Ochoa, M. E.; Santillan, R.; Farfán, N.; Garcia-Garibay, M. A. *RSC Adv.* **2015**, *5*, 55201–55208. (e) Jiang, X.; O'Brien, Z. J.; Yang, S.; Lai, L. H.; Buenaflor, J.; Tan, C.; Khan, S.; Houk, K. N.; Garcia-Garibay, M. A. *J. Am. Chem. Soc.* **2016**, *138*, 4650–4656.
- (6) (a) Setaka, W.; Yamaguchi, K. *J. Am. Chem. Soc.* **2013**, *135*, 14560–14563, and earlier work cited therein. (b) Setaka, W.; Inoue, K.; Higa, S.; Yoshigai, S.; Kono, H.; Yamaguchi, K. *J. Org. Chem.* **2014**, *79*, 8288–8295. (c) Shionari, H.; Inagaki, Y.; Yamaguchi, K.; Setaka, W. *Org. Biomol. Chem.* **2015**, *13*, 10511–10516. (d) Nishiyama, Y.; Inagaki, Y.; Yamaguchi, K.; Setaka, W. *J. Org. Chem.* **2015**, *80*, 9959–9966.
- (7) Shima, T.; Hampel, F.; Gladysz, J. A. *Angew. Chem., Int. Ed.* **2004**, *43*, 5537–5540; *Angew. Chem.* **2004**, *116*, 5653–5656.
- (8) (a) Nawara, A. J.; Shima, T.; Hampel, F.; Gladysz, J. A. *J. Am. Chem. Soc.* **2006**, *128*, 4962–4963. (b) Nawara-Hultzs, A. J.; Stollenz, M.; Barbasiewicz, M.; Szafert, S.; Lis, T.; Hampel, F.; Bhuvanes, N.; Gladysz, J. A. *Chem. - Eur. J.* **2014**, *20*, 4617–4637. (c) Taher, D.; Nawara-Hultzs, A. J.; Bhuvanes, N.; Hampel, F.; Gladysz, J. A. *J. Organomet. Chem.* **2016**, DOI: 10.1016/j.jorganchem.2016.03.022.
- (9) Wang, L.; Hampel, F.; Gladysz, J. A. *Angew. Chem., Int. Ed.* **2006**, *45*, 4372–4375; *Angew. Chem.* **2006**, *118*, 4479–4482.
- (10) (a) Wang, L.; Shima, T.; Hampel, F.; Gladysz, J. A. *Chem. Commun.* **2006**, 4075–4077. (b) Estrada, A. L.; Jia, T.; Bhuvanes, N.; Blümel, J.; Gladysz, J. A. *Eur. J. Inorg. Chem.* **2015**, *2015*, 5318–5321.
- (11) Heß, G. D.; Hampel, F.; Gladysz, J. A. *Organometallics* **2007**, *26*, 5129–5131.
- (12) Skopek, K.; Gladysz, J. A. *J. Organomet. Chem.* **2008**, *693*, 857–866.
- (13) Zeits, P. D.; Rachiero, G. P.; Hampel, F.; Reibenspies, J. H.; Gladysz, J. A. *Organometallics* **2012**, *31*, 2854–2877.
- (14) (a) Fiedler, T.; Bhuvanes, N.; Hampel, F.; Reibenspies, J. H.; Gladysz, J. A. *Dalton Trans.* **2016**, *45*, 7131–7147. (b) Fiedler, T.; Chen, L.; Wagner, N. D.; Russell, D. R.; Gladysz, J. A. *Organometallics* **2016**, *35*, DOI: 10.1021/acs.organomet.6b00249.
- (15) See <http://www.gyroscopes.org/uses.asp>. The authors are unaware of any books or peer reviewed articles that match the diversity of examples on this web site, which is maintained by G. Turner.
- (16) Zheng, X.; Mulcahy, M. E.; Horinek, D.; Galeotti, F.; Magnera, T. F.; Michl, J. *J. Am. Chem. Soc.* **2004**, *126*, 4540–4542 and references therein.
- (17) (a) Butikov, E. *Eur. J. Phys.* **2006**, *27*, 1071–1081. (b) Kleppner, D.; Kolenkow, R. J. *An Introduction to Mechanics*; Cambridge University Press: Cambridge, 2010; Chapters 7.3–7.5.
- (18) (a) Lang, G. M.; Skaper, D.; Shima, T.; Otto, M.; Wang, L.; Gladysz, J. A. *Aust. J. Chem.* **2015**, *68*, 1342–1351. (b) A reviewer has requested a brief explanation of the missing index  $d$  for  $m = 7$  ( $n = 16$ ). Since complexes of the phosphine  $\text{P}((\text{CH}_2)_7\text{CH}=\text{CH}_2)_3$  have been synthesized,<sup>14a</sup> it seems helpful to assign a sequential letter to each methylene chain length.
- (19) (a)  $\text{Ru}(\text{=CHPh})(\text{PCy}_3)_2(\text{Cl})_2$ . (b)  $\text{Ru}(\text{=CHPh})(\text{H}_2\text{IMes})(\text{PCy}_3)(\text{Cl})_2$ ,  $\text{H}_2\text{IMes} = 1,3\text{-dimesityl-4,5-dihydroimidazol-2-ylidene}$ .
- (20) Shima, T.; Bauer, E. B.; Hampel, F.; Gladysz, J. A. *Dalton Trans.* **2004**, 1012–1018.
- (21) (a) Garrou, P. E. *Chem. Rev.* **1981**, *81*, 229–266. (b) Gorenstein, D. G. *Phosphorus-31 NMR-Principles and Applications*; Academic Press, Inc.: Orlando, FL, 1984; Chapter 1. (c) The variation with ring size has been analyzed in terms of shift tensor components. Lindner, E.; Fawzi, R.; Mayer, H. A.; Eichele, K.; Hiller, W. *Organometallics* **1992**, *11*, 1033–1043.
- (22) The  $J$  values given for virtual triplets or multiplets approximating doublets of doublets represent the apparent couplings and not the mathematically rigorous coupling constants. Hersch, W. H. *J. Chem. Educ.* **1997**, *74*, 1485–1488.



- (23) Resonances were assigned as follows. First, the  $\text{PCH}_2\text{CH}_2\text{CH}_2$   $^1\text{H}$  NMR signals of  $E,E,E$ -3a and  $5\text{C}^+\text{BF}_4^-$  were identified via  $^1\text{H}, ^1\text{H}$  COSY experiments. The  $\text{PCH}_2\text{CH}_2\text{CH}_2$   $^{13}\text{C}$  signals were then identified by  $^1\text{H}, ^{13}\text{C}$  HSQC experiments. The coupling constant and chemical shift trends thus established were used to assign the  $\text{PCH}_2\text{CH}_2\text{CH}_2$  signals of the other complexes. Analogous spectra for related complexes can be found in refs 14a and 57.
- (24) Boddien, A.; Gärtner, F.; Jackstell, R.; Junge, H.; Spannenberg, A.; Baumann, W.; Ludwig, R.; Beller, M. *Angew. Chem., Int. Ed.* **2010**, *49*, 8993–8996; *Angew. Chem.* **2010**, *122*, 9177–9181.
- (25) Since the three  $\text{FeCQ}$  distances are usually within experimental error or “three esd values”, the average, as opposed to the longest, is employed.
- (26) (a) Bondi, A. J. *Phys. Chem.* **1964**, *68*, 441–451. The van der Waals radii of  $\text{sp}^3$  and  $\text{sp}^2$  carbon atoms are identical (1.70 Å); for simplicity, the same value is applied to CO carbon atoms. (b) Mantina, M.; Chamberlin, A. C.; Valero, R.; Cramer, C. J.; Truhlar, D. G. *J. Phys. Chem. A* **2009**, *113*, 5806–5812.
- (27) For example, since the carbon chains are conformationally mobile in solution, it may be more appropriate to take an average distance for  $\text{Fe}-\text{C}^{\text{distal}}$ .
- (28) (a) Johnson, B. F. G.; Segal, J. A. *J. Chem. Soc., Dalton Trans.* **1972**, 1268–1271. See also (b) Touchard, D.; Le Bozec, H.; Dixneuf, P. *Inorg. Chim. Acta* **1979**, *33*, L141–L142. (c) Ahmed, F. R.; Roustan, J. L. A.; Al-Janabi, M. Y. *Inorg. Chem.* **1985**, *24*, 2526–2532. (d) Crooks, G. R.; Johnson, B. F. G. *J. Chem. Soc. A* **1968**, 1238–1240.
- (29) (a) Ashford, P. K.; Baker, P. K.; Connelly, N. G.; Kelly, R. L.; Woodley, V. A. *J. Chem. Soc., Dalton Trans.* **1982**, 477–479, and earlier work referenced therein. (b) Richter-Addo, G. B.; Legzdins, P. *Metal Nitrosyls*; Oxford University Press, Inc.: New York, 1992; Chapter 2, pp 37–38. (c) Connelly, N.; Geiger, W. E. *Chem. Rev.* **1996**, *96*, 877–910.
- (30) Kochi, J. K. *J. Organomet. Chem.* **1986**, *300*, 139–166.
- (31) Sowa, J. R., Jr.; Zanolli, V.; Facchin, G.; Angelici, R. J. *J. Am. Chem. Soc.* **1991**, *113*, 9185–9192.
- (32) Brookhart, M.; Grant, B.; Volpe, A. F. *Organometallics* **1992**, *11*, 3920–3922.
- (33) The  $\text{IR } \nu_{\text{MH}}$  bands are, by analogy to those of the osmium hydride complexes *mer, trans*- $[\text{Os}(\text{H})(\text{CO})_3(\text{PR}_3)_2]^+\text{Z}^-$ , expected to be much weaker than the  $\nu_{\text{CO}}$  bands (and at lower frequencies). Laing, K. R.; Roper, W. R. *J. Chem. Soc. A* **1969**, 1889–1891. See also Franke, O.; Wiesler, B. E.; Lehnert, N.; Tuzcek, F. Z. *Anorg. Allg. Chem.* **2002**, *628*, 2395–2402.
- (34) Siegel, J. S.; Anet, F. A. L. *J. Org. Chem.* **1988**, *53*, 2629–2630.
- (35) Budzelaar, P. H. M. *gNMR: NMR Simulation Program*, version 5.0.6.0; Adept Scientific: Luton, U.K., 2006.
- (36) Karlen, S. D.; Garcia-Garibay, M. A. *Top. Curr. Chem.* **2005**, *262*, 179–227.
- (37) Fyfe, C. A. *Solid-State NMR for Chemists*; CFC Press: Guelph, Ontario, Canada, 1983; pp 199–209.
- (38) Duncan, T. M. *A Compilation of Chemical Shift Anisotropies*; Farragut Press: Chicago, IL, 1990; p C-35.
- (39) Cluff, K. J.; Bhuvanesh, N.; Blümel, J. *Chem. - Eur. J.* **2015**, *21*, 10138–10148.
- (40) The program “dmfit” was applied. Massiot, D.; Fayon, F.; Capron, M.; King, I.; Le Calvé, S.; Alonso, B.; Durand, J.-O.; Bujoli, B.; Gan, Z.; Hoatson, G. *Magn. Reson. Chem.* **2002**, *40*, 70–76.
- (41) Hilliard, C. R. Doctoral dissertation, Texas A&M University, College Station, TX, 2013.
- (42) Kirkland, T. A.; Grubbs, R. H. *J. Org. Chem.* **1997**, *62*, 7310–7318.
- (43) (a) Conrad, J. C.; Eelman, M. D.; Silva, J. A. D.; Monfette, S.; Parnas, H. H.; Snelgrove, J. L.; Fogg, D. E. *J. Am. Chem. Soc.* **2007**, *129*, 1024–1025. (b) Monfette, S.; Fogg, D. E. *Chem. Rev.* **2009**, *109*, 3783–3816.
- (44) Bauer, E. B.; Hampel, F.; Gladysz, J. A. *Organometallics* **2003**, *22*, 5567–5580.
- (45) Almenningsen, A.; Anfinsen, I. M.; Haaland, A.; Jerslev, B.; Schäffer, C. E.; Sunde, E.; Sørensen, N. A. *Acta Chem. Scand.* **1970**, *24*, 43–49.
- (46) Lee, C. W.; Grubbs, R. H. *Org. Lett.* **2000**, *2*, 2145–2147.
- (47) (a) Albers, M. O.; Coville, N. J. *Coord. Chem. Rev.* **1984**, *53*, 227–259. (b) Luh, T.-Y. *Coord. Chem. Rev.* **1984**, *60*, 255–276.
- (48) Pankowski, M.; Bigorgne, M. J. *Organomet. Chem.* **1971**, *30*, 227–234.
- (49) (a) Fischer, E. O.; Kiener, V. J. *Organomet. Chem.* **1970**, *23*, 215–233. (b) For derivatization protocols, see Semmelhack, M. F.; Tamura, R. J. *Am. Chem. Soc.* **1983**, *105*, 4099–4100.
- (50) Scherer, A. Doctoral dissertation, Universität Erlangen-Nürnberg, Erlangen, Germany, 2009; Chapter 4.
- (51) (a) Tam, W.; Lin, G.-Y.; Wong, W.-K.; Kiel, W. A.; Wong, V. K.; Gladysz, J. A. *J. Am. Chem. Soc.* **1982**, *104*, 141–152. (b) Tam, W.; Lin, G.-Y.; Gladysz, J. A. *Organometallics* **1982**, *1*, 525–529.
- (52) Liu, L.; Guo, Q.-X. *Chem. Rev.* **2001**, *101*, 673–696.
- (53) Marahatta, A. B.; Kanno, M.; Hoki, K.; Setaka, W.; Irle, S.; Kono, H. *J. Phys. Chem. C* **2012**, *116*, 24845–24854.
- (54) Commings, P.; Nuñez, J. E.; Garcia-Garibay, M. A. *J. Org. Chem.* **2011**, *76*, 8355–8363.
- (55) (a) Karlen, S. D.; Ortiz, R.; Chapman, O. L.; Garcia-Garibay, M. A. *J. Am. Chem. Soc.* **2005**, *127*, 6554–6555. (b) Czajkowska-Szczykowska, D.; Rodríguez-Molina, B.; Magaña-Vergara, N. E.; Santillan, R.; Morzycki, J. W.; Garcia-Garibay, M. A. *J. Org. Chem.* **2012**, *77*, 9970–9978.
- (56) Iron tetracarbonyl phosphine and arsine complexes of the formula  $\text{Fe}(\text{CO})_4(\text{E}(\text{o-tol})_3)$  have been crystallographically characterized. The  $\text{Fe}-\text{As}$  bond is 3.6% longer than the  $\text{Fe}-\text{P}$  bond; see (a) Howell, J. A. S.; Palin, M. G.; McArdle, P.; Cunningham, D.; Goldschmidt, Z.; Gottlieb, H. E.; Hezroni-Langerman, D. *Inorg. Chem.* **1991**, *30*, 4683–4685. (b) Howell, J. A. S.; Palin, M. G.; McArdle, P.; Cunningham, D.; Goldschmidt, Z.; Gottlieb, H. E.; Hezroni-Langerman, D. *Inorg. Chem.* **1993**, *32*, 3493–3500. (c) The  $\text{Fe}-\text{As}$  bonds in closely related iron tricarbonyl complexes with *cis*  $\text{As}-\text{Fe}-\text{As}$  and  $\text{P}-\text{Fe}-\text{P}$  linkages are 6.6–3.8% longer: Brown, D. S.; Bushnell, G. W. *Acta Crystallogr.* **1967**, *22*, 296–299. Hogarth, G. *J. Organomet. Chem.* **1991**, *406*, 391–398.
- (57) Lang, G. M.; Bhuvanesh, N.; Reibenspies, J. H.; Gladysz, J. A. submitted to *Organometallics*.
- (58) (a) Bermudez, V.; Capron, N.; Gase, T.; Gatti, F. G.; Kajzar, F.; Leigh, D. A.; Zerbetto, F.; Zhang, S. *Nature* **2000**, *406*, 608–611. (b) Horansky, R. D.; Clarke, L. I.; Price, J. C.; Khuong, T.-A. V.; Jarowski, P. D.; Garcia-Garibay, M. A. *Phys. Rev. B: Condens. Matter Mater. Phys.* **2005**, *72*, 014302. (c) Horansky, R. D.; Clarke, L. I.; Winston, E. B.; Price, J. C.; Karlen, S. D.; Jarowski, P. D.; Santillan, R.; Garcia-Garibay, M. A. *Phys. Rev. B: Condens. Matter Mater. Phys.* **2006**, *74*, 054306. (d) Dhar, P.; Swayne, C. D.; Fischer, T. M.; Kline, T.; Sen, A. *Nano Lett.* **2007**, *7*, 1010–1012. (e) Arcenegui, J. J.; García-Sánchez, P.; Morgan, H.; Ramos, A. *Phys. Rev. E* **2013**, *88*, 033025.
- (59) Lang, G. M.; Skaper, D.; Hampel, F.; Gladysz, J. A. to be submitted for publication.
- (60) Data were treated as recommended by Cammenga, H. K.; Epple, M. *Angew. Chem., Int. Ed. Engl.* **1995**, *34*, 1171–1187; *Angew. Chem.* **1995**, *107*, 1284. The  $T_c$  values best represent the temperature of the phase transition.
- (61) This melting point was determined under argon using a sample that had been washed with hexane prior to drying. Two independently prepared samples that were not so-treated showed darkening and shrinkage at ca. 50 °C.
- (62) FAB, 3-NBA,  $m/z$  (relative intensity, %); the most intense peak of the isotope envelope is given.
- (63) These data do not indicate an analytically pure sample but are provided nonetheless to illustrate the best fit obtained to date.
- (64) (a) Nonius, B. V. *Collect*, data collection software; 1998. (b) Otwinowski, Z. *Scapecap*, data processing software; HKL Research, Inc.: Charlottesville, VA, 1985. See also Otwinowski, Z.; Minor, W. *Methods Enzymol.* **1997**, *276*, 307.
- (65) Sheldrick, G. M. *Acta Crystallogr., Sect. A: Found. Crystallogr.* **2008**, *64*, 112–122.
- (66) Cromer, D. T.; Waber, J. T. In *International Tables for X-ray Crystallography*; Ibers, J. A., Hamilton, W. C., Eds.; Kynoch: Birmingham, U.K., 1974.
- (67) Dolomanov, O. V.; Bourhis, L. J.; Gildea, R. J.; Howard, J. A. K.; Puschmann, H. *J. Appl. Crystallogr.* **2009**, *42*, 339–341.